



UNIVERSITÀ POLITECNICA DELLE MARCHE
Repository ISTITUZIONALE

Assessing the flood risk to evacuees in outdoor built environments and relative risk reduction strategies

This is the peer reviewed version of the following article:

Original

Assessing the flood risk to evacuees in outdoor built environments and relative risk reduction strategies / Bernardini, G.; Finizio, F.; Postacchini, M.; Quagliarini, E.. - In: INTERNATIONAL JOURNAL OF DISASTER RISK REDUCTION. - ISSN 2212-4209. - ELETTRONICO. - 64:(2021). [10.1016/j.ijdr.2021.102493]

Availability:

This version is available at: 11566/291669 since: 2024-04-30T14:37:48Z

Publisher:

Published

DOI:10.1016/j.ijdr.2021.102493

Terms of use:

The terms and conditions for the reuse of this version of the manuscript are specified in the publishing policy. The use of copyrighted works requires the consent of the rights' holder (author or publisher). Works made available under a Creative Commons license or a Publisher's custom-made license can be used according to the terms and conditions contained therein. See editor's website for further information and terms and conditions.

This item was downloaded from IRIS Università Politecnica delle Marche (<https://iris.univpm.it>). When citing, please refer to the published version.

note finali coverpage

(Article begins on next page)

POSTPRINT OF Bernardini G, Finizio F, Postacchini M, Quagliarini E (2021) Assessing the flood risk to evacuees in outdoor built environments and relative risk reduction strategies. *International Journal of Disaster Risk Reduction* 64:102493. <https://doi.org/10.1016/j.ijdrr.2021.102493>

Highlights

- Flood risk evaluation and **reduction** in **outdoor** built environments are investigated.
- **The proposed behavioural design-based** approach **jointly considers** evacuation **and** hydrodynamic scenarios
- Novel Key Performance Indicators are proposed
- Such approach is applied to a significant case study
- Risk **reduction** strategies are proposed and their effectiveness evaluated

1 **Assessing the flood risk to evacuees in outdoor built environments and relative** 2 **risk reduction strategies**

3 Gabriele Bernardini¹, Fiorenza Finizio², Matteo Postacchini², Enrico Quagliarini^{1,*}

4

5 ¹ DICEA Dept, Università Politecnica delle Marche, via Brecce Bianche 60131 Ancona

6 phone: +39 071 220 4248, mail: g.bernardini@univpm.it; e.quagliarini@univpm.it

7 ² DICEA Dept, Università Politecnica delle Marche, via Brecce Bianche 60131 Ancona

8 phone: +39 071 220 4539, mail: m.postacchini@univpm.it

9

10 *Corresponding author: e.quagliarini@univpm.it; phone: +39 071 220 4248

11 **Abstract**

12 Climate-change induced disasters, like floods, are expected to increase in the future. In outdoor built environments, **flood**
13 **risk to evacuees** depends on interactions between floodwater spreading, built environment features, flood-induced
14 modifications, and individuals' reaction in emergency phases. Disaster risk reduction strategies should mitigate the
15 immediate flood impacts and improve the community resilience, while being easy-to-implement and effectively
16 supporting evacuees during the initial phases of the emergency. Simulation-based methodologies could support safety
17 planners in evaluating the effectiveness of such strategies, especially if basing on a micro-scale-oriented approach that
18 represents emergency interactions between each individual and the surrounding outdoor built environment. This study
19 adopts an existing micro-scale simulator (FloopEDS) reproducing experimental-based flood evacuation behaviours.
20 According to a behavioural design-based approach, **simulation** results focus on individual responses in the outdoor built
21 environment through Key Performance Indicators (KPIs) aimed at providing evidence of critical interactions between
22 evacuees, floodwaters and the outdoor built environment. A case study is selected by considering different flood scenarios
23 to test such KPIs. Risk reduction solutions are then provided, and their effectiveness is checked by simulations. Results
24 show the micro-scale and behavioural design-based approach capabilities in proposing multi-scenarios solutions (e.g.:
25 architectural elements to support evacuees; emergency planning).

26

27 **Keywords:** flood risk; flood evacuation; risk assessment and planning; behavioural design; risk reduction strategies; flood
28 hydrodynamics.

29 **1 Introduction**

30 Climate change-induced disasters, such as floods, are significantly affecting built environments and their probability
31 is expected to increase in the future. Thus, disaster risk reduction, **which** is the series of activities aimed at preventing
32 new and reducing existing disaster risk and managing residual risk¹, is a key challenge for guaranteeing the safety of our
33 communities, especially those placed in urban built environments [1–5]. Floods represent one of the most important dis-
34 asters in existing and future cities, because of their effects on the built environment (defined as a system of buildings,
35 underground spaces, open spaces such as streets and squares) and the people who live in them [3,6–13]. Flood risk as-
36 sessment and reduction in urban areas are usually based on three factors [2,7,14–16]:

- 37 • Site hazard, due to both probability of occurrence of flood and location of urban areas in risk-prone regions;
- 38 • The vulnerability of the built environment to floodwater;
- 39 • Community’s exposure, addressed in terms of exposed people (number and characterization) and social-eco-
40 nomic factors.

41 In this general context, the evacuation and loss of life modelling in flood-affected urban scenarios was widely
42 undertaken by previous studies in the last 15 years, due to the critical issues for individuals’ safety that appear during the
43 initial phases of such an emergency [17–25]. In fact, although safety planners can usually assume that exposed individuals
44 know “what they must do” and “where they must go”, recent research has demonstrated that this assumption is incorrect
45 [26]. During an evacuation, exposed individuals are affected by their own and the floodwaters interaction with the built
46 environment. In addition, some of them could engage in “risky behaviours” during flood events, such as wasting time or
47 trying to cross areas of fast-flowing and/or deep water.

48 These phenomena are relevant especially considering urban city **centres** because the number of exposed individuals is
49 higher than in other **environments at risk of flooding** [8,16,22,24,27,28]. Furthermore, in urban areas, buildings can have
50 a significant impact on floodwater depths and velocities [11,16,29,30]. For instance, where buildings are close together
51 and roads are narrow, this can increase the velocity and depth of the floodwater thus increasing the flood hazard. In

¹ <https://www.undrr.org/terminology/disaster-risk-reduction> , last access 12/04/2021

52 addition to damages to buildings and goods [2,7], the following conditions can increase the risk to exposed people
53 [10,11,17,20,22,27,31–34]:

- 54 1. people are located in the outdoor built environment (e.g. the open spaces such as streets, squares) or in
55 underground spaces (e.g. metro systems) at the beginning of the flood event;
- 56 2. people are evacuating in outdoor areas during the flood;
- 57 3. when people are not allowed to reach safer places inside a building adjacent to a flooded street.

58 These scenarios imply more significant threats for people due to the possibility to evacuate and to maintain stability
59 while moving, and affect the overall number of casualties, especially in outdoor built environments [18,21,28,35–38].
60 Technicians of local authorities and Civil Protection Bodies can adopt Decision Support Systems (DSS) and related
61 simulation tools for risk assessment purposes and for suggesting reliable risk reduction strategies [15,22,28,39–42].
62 Following such demand, many DSS and modelling tools have been provided over the time [9,11,20,24,25,28]. They have
63 moved towards the inclusion of behavioural aspects characterizing experimental-based individual-floodwater
64 interactions, so as to pursue reliable simulation and assessment approaches focusing on the evacuees' safety analysis as a
65 paramount issue for flood risk [1,9,17,19,20,22,42].

66

67 **1.1 Modelling flood evacuation for risk assessment and risk reduction strategies**

68 The analysis of real-world flood evacuations outlined significant differences between behaviours in flood emergencies
69 and **other** kinds of disasters (like earthquake, fire, general-purpose) [35,37,43]. From a qualitative point of view, evacuees
70 are more likely to move toward immobile objects such as buildings, fences, handrails, during floods, unlike during other
71 kinds of disasters [17,35,37,44–47]. Meanwhile, social identification issues lead evacuees to remain close to other neigh-
72 bouring **individuals and** to share evacuation path decisions between evacuees in the same group. From a quantitative point
73 of view, experimental activities (with volunteers or mannequins) mainly demonstrated that water depth D [m] and speed
74 V [m] are key factors affecting the evacuees' motion on foot [21,37,48,49]. Individual features in terms of height, body
75 mass, age and gender affect both the motion speed and the stability in floodwaters [21,22,38]. General rules were set to
76 correlate floodwater characteristics and individuals' speed [48,49], as well as human body stability criteria for buoyancy
77 or body failure (sliding and toppling under floodwaters effects) [35,38,50–52]. Such results show that flood risk assess-
78 ment needs the adoption of models based on specific flood evacuation behaviours and related motion quantities, as sug-
79 gested by behavioural design-based perspectives pursued by recent works [26,43]. Meanwhile, micro-scale modelling

80 approaches [22,53] can be preferred because they are able to represent these experimentally-based behaviours for each
81 involved evacuee. In this sense, results from recent works, e.g. concerning $D-V$ correlations, have been introduced in
82 micro-scale pedestrian evacuation simulators and their capabilities have been thus demonstrated [17,18,22,25,54].

83 As for other kinds of disasters (e.g. earthquake, fire, tsunami) affecting the built environment [55–58], this behavioural
84 design-based and micro-scale approach can support the development of flood emergency and evacuation simulators
85 [22,26,43]. Safety designers can use these tools while performing risk assessment actions to evaluate the probable safety
86 levels for evacuees. In particular, the response of “each individual receptor at risk” [24] can be assessed depending on the
87 surrounding hazardous conditions each evacuee should face while moving in the flooded environment. Thus, risk reduc-
88 tion strategies aimed at supporting each individual in emergency conditions can be defined and promoted. Combined
89 hydrodynamic-pedestrian evacuation simulators are used to this end [17,18,22,59]. The hydrodynamic model is aimed at
90 reproducing the time evolution of the floodwater spreading (i.e. speed and depth) depending on the type of flood and the
91 layout of the built environment [29,30]. The evacuation model represents individuals’ interactions with floodwaters,
92 emergency behaviours and choices of the evacuees, depending on surrounding floodwater conditions [18,22,48].

93 Simulation results are then analysed by Key Performance Indicators (KPIs) to evaluate the safety levels of the evacuees
94 in the emergency process [3,16,24,42,60]. Time-dependend risk assessment indices and GIS-based implementation were
95 provided [10,34], while additional works also included KPIs relating to flood damage assessment of the built environment
96 [2,16,41,61]. Considering behavioural design-based KPIs, evacuation models are widely used to estimate evacuation tim-
97 ing and the loss of life in the urban spaces, according to different Life Safety Models and hazard or risk rating metrics
98 [10,11,22,34,54,62]. However, additional aspects of the evacuation process which are generally assessed by other kinds
99 of evacuations (e.g. fire safety, earthquake), should be included in risk assessment analysis for the definition of risk
100 indices in the outdoor built environment, such as the evacuation curve/flows, the use of open spaces, the presence of
101 spontaneous gathering areas [1,17–19,56].

102 Outputs from the macro (territorial or urban) to the micro (building, street, square, underground space) scales are used
103 for KPI-based evaluation of the effectiveness of risk reduction strategies aimed at reducing probable outcoming emer-
104 gency interferences between the evacuees and the surrounding conditions by [1,17,19,22,24,27]:

- 105 • implementing modifications to the built environment, such as those relating to building components, emergency
106 path configurations, and building systems as countermeasures during the flood;
- 107 • providing exposed people with information such as how to react when they receive a flood warning, where to go in
108 case of an evacuation or which flood risk level can occur in the urban spaces, by also using emergency and
109 wayfinding signage systems;

110 • adapting emergency management strategies to give direct support to evacuees (i.e. position of gathering areas;
111 shelters allocation and relief distribution), if other “preventive” risk reduction solutions (e.g. flood barriers, drainage
112 systems, early warning systems) fail.

113 Furthermore, reliable and widespread micro-scale solutions concerning the built environment elements were provided,
114 including, for instance, stability-increasing solutions such as street furniture and handrails, or areas where to gather and
115 wait for the rescuers’ arrival, such as raised platforms² [35,37,45]. Nevertheless, the assessment of their capabilities should
116 be investigated in an organized manner through a KPIs-based approach and considering their impact from both micro and
117 macro-scales.

118 1.2 Work aims and proposed approach

119 This work provides a micro-scale-oriented and behavioural design-based methodology for the assessment of flood risk
120 and the evaluation of risk reduction strategies in outdoor built environments, focusing on open spaces such as streets and
121 squares. The methodology investigates the initial phases of a flood emergency, that is the evacuation. According to this
122 micro-scale standpoint [24], the proposed methodology is based on the joint simulation of hydrodynamic conditions and
123 evacuation behaviours of each individual at risk, over space and time. Experimental-based flood evacuation behaviours
124 are included in the evacuation simulation model. KPIs are provided to consider the effects of the interactions between
125 each individual and the conditions of surrounding floodwaters and the outdoor built environment, at the: 1) micro-scale,
126 that is for each street and square composing the analysed built environment, thus identifying homogenous risk areas; 2)
127 macro-scale, that is for the whole outdoor built environment. Finally, the work proposes risk reduction solutions focused
128 on micro-scale interventions that can [9,26,27,42,63]: a) directly support individuals in emergency conditions; b) be easily
129 implemented and architecturally integrated into the outdoor built environment; c) have a sustainable use also in non-
130 disaster conditions.

131 This whole approach is applied to the city centre of Senigallia (Italy), recently hit by a flood induced by long-duration
132 rainfall and levee-failure [16]. Thanking the application to this case study, this work wants to mainly demonstrate the
133 capabilities of the proposed risk assessment and risk reduction methodology, rather than deeply represent a specific real-
134 world scenario.

135

² see <https://www.rogersarchitects.com/mta-flood-mitigation-street-furniture/> for an example of architecturally-integrated solutions in urban areas (last access: 11/03/2021)

136 2 Phases and methods

137 This work was organized in three main phases. In the first phase, according to the micro-scale and behavioural design-
138 based approach, criteria for emergency simulations were defined through the use of an existing hydrodynamic-evacuation
139 simulator (Section 2.1). In the second phase, behavioural design-based KPIs were defined to evaluate risk levels in flood
140 scenarios and propose risk reduction strategies (Section 2.2). Finally, a case study application was provided (Section 2.3)
141 by analyzing different flood scenarios. Then, risk reduction strategies were proposed and verified by considering the
142 riskiest scenario.

143 2.1 Simulation modelling

144 The combined simulator (FloopEDS) is based on a hydrodynamic model which simulates floodwater conditions in an
145 urban environment and a behavioural model which reproduces evacuees' choices (for details, see [17])³. The hydrody-
146 namic model is based on the Nonlinear Shallow Water Equations (NSWEs hereafter). It is generally used for the repre-
147 sentation of shallow water problems, that typically occur in the coastal area, in rivers or open channels, in the urban
148 environment [64]. The behavioural model for evacuation relies on previous work providing a complete overview of or-
149 ganized evacuation behaviours during flood [37]. Starting from literature outcomes, this work included empirical analyses
150 on real flood emergencies and proposed their related general rules for simulation. These rules were implemented in a
151 micro-scale agent-based modelling approach, namely the Social Force Model (SFM) [65]. The SFM was adopted to de-
152 scribe the individual's motion in the built environment. In the SFM, attractive and repulsive forces are applied to each
153 simulated individual to represent interactions among them and with the built environment, by also including: 1) attraction
154 forces between the individuals and immobile objects in the built environment; 2) effects of individuals' speed reduction
155 due to floodwaters D and V . The complete model description and the model notations are provided in Appendix A. A
156 summary of the main modelling criteria is discussed in this section.

157 Firstly, it is considered that the maximum simulation time depends on the hydrodynamic conditions. In particular,
158 when (almost) steady conditions within the domain are reached, the evacuation simulation can end. In fact, beyond this
159 time limit, the evacuation conditions are not affected by variations in the hydrodynamic conditions during the time.

160 The hydrodynamic model provides the time evolution of water depth $D(x,y,t)$ and depth-averaged flow speed $V(x,y,t)$
161 in the outdoor built environment, where evacuees move. Two parameters can be defined, i.e. the specific force per unit

³ The executable file for the behavioural model ("beta version") is available in the journal supplementary materials, by including the case study scenario inputs and output dataset presented by this work.

162 width $M(x,y,t)$ [m^3/m] = $(D \cdot V^2)/g + D^2/2$ (where g is the gravity acceleration [9.81m/s^2]) and the descriptor of critical
163 surrounding conditions for human body stability $DV(x,y,t) = D(x,y,t) \cdot V(x,y,t)$ [m^2/s] [18,35,38,48]. The SFM-based simu-
164 lator for the evacuation process uses these inputs to determine [17,37,38]:

- 165 • the evacuees' speed depending on M ;
- 166 • his/her possibility of body stability loss, depending on DV ;
- 167 • the path choices, to minimize the M values and the distance towards a safe area where he/she can gather.

168 At the end of the simulation, the model provides data on:

- 169 • the *arrived evacuees*, as the individuals who gained a safe area;
- 170 • the *latecomers*, as the individuals (located along the outdoor built environment) who are still moving towards
171 a safe area;
- 172 • *spontaneously gathering evacuees*, as the individuals who spontaneously gather in groups in areas where M
173 values are lower than the ones of the surrounding outdoor spaces;
- 174 • the *casualties*, by considering the individuals who are exposed to floodwater conditions where they become
175 unstable ($DV > 1.20 \text{ m}^2/\text{s}$). In addition, the other thresholds for adults in good conditions having a height (h_i)
176 and mass (m_i) product $h_i m_i > 50$, that are $D(x,y,t) < 1.2\text{m}$ and $V(x,y,t) < 3.2\text{m/s}$, are still considered valid [31,38].

177 More details are offered in Appendix A.

178 The model considers a gaussian distribution for $v_{pref,t}(x,y,t)$ (calculated as function of $M(x,y,t)$) considering a stand-
179 ard deviation of 0.2m/s [49,66]. In addition, an error for path selection (10%) is assumed to represent the evacuees who
180 do not decide to select a safe area as an evacuation target because of safer local conditions [37,59]. Therefore, the evacu-
181 ation process in each scenario is simulated more than once, and the mean values (and related standard deviation) are
182 calculated [53,67]. For each scenario, the convergence of simulated behaviours is considered reached if the standard
183 deviation associated with each output is lower than 10% [17]. At least 5 simulations per scenario have been run.

184 It is worthy of notice that the behavioural model assumptions imply some limitations concerning rules for the simu-
185 lation of evacuees' speeds and stability in floodwater. In fact, this work is mainly focused on demonstrating the capabil-
186 ities of the proposed micro-scale and behavioural design-based approach, rather than on representing specific individual
187 features or case study conditions. We simulated the evacuation of adults (having $h_i m_i > 50$) homogeneously defined [38],
188 thus ignoring additional risk affecting individual features. Their safety threshold for stability is homogeneously consid-
189 ered too, thus focusing on the average response of such kind of evacuees. Specific individuals' features such as height,

190 body mass, age, gender or motion abilities, that affect both speeds and stability [21,22,49], were then not considered in
191 the current simulations.

192 **2.2 Behavioural Key Performance Indicators for scenarios comparisons and criteria for risk reduction** 193 **strategies**

194 Simulations were performed in different “*flood scenarios*” and “*risk reduction scenarios*”. Thus, KPIs compared the
195 simulation results by considering [18,56,57]:

- 196 **1.** different **open spaces (such as streets and squares)** in the outdoor built environment, within the same “*flood*
197 *scenario*”, to **point out** where to implement possible risk reduction strategies;
- 198 **2.** different “*risk reduction scenarios*”, to evaluate their improvement of safety conditions.

199 Two groups of KPIs were proposed. *KPIs relating to the evacuation process* (Section 2.2.1) represent the effects of
200 individual-floodwater interactions on the evacuation. According to the stochastic evacuation simulation approach de-
201 scribed in Section 2.1, each KPI was estimated on the simulation outputs and then it was associated at least to its average
202 value and its standard deviation. *KPIs relates to the built environment* (the whole simulation area or a part of it, e.g. a
203 street or a square) trace the risk levels depending on the specific floodwater characterization and **the adopted** risk reduction
204 strategies (Section 2.2.2). The KPIs notations are provided in Appendix B.

205 **2.2.1 KPIs relating to the evacuation process**

206 The overall *number of evacuees who have arrived in a safe area within the simulation time* P_e [persons] describes the
207 number of people who can reach effective safe conditions within the simulation time. This KPI can be also represented
208 in percentage terms $P_{e,\%}$ [%], with respect to the initial people hosted in the outdoor built environment. P_e should be
209 maximized to improve the **evacuees’** safety [35,57,68,69]. P_e related to each safe area in the built environment assesses
210 if it is underused/not used at all by the evacuees. The *difference in arriving evacuees* [%] describes the use of each safe
211 areas depending on the individuals’ selection of paths and safe areas. In fact, some individuals can spontaneously try to
212 move towards a safe area different from the initially selected one because of local floodwater levels conditions [37], as
213 reported in the model description in Appendix A. Thus, the *difference in arriving evacuees* [%] was calculated as the
214 percentage difference between the number of evacuees reaching the safe area and the number of evacuees who “initially
215 chose” the safe area.

216 The *evacuation time* T_e [s] is linked to P_e [18,70]. The *average evacuation time* $T_{e,0.50}$ refers to the 50th percentile of
217 evacuation **time and represents the median trend in the evacuation process**. According to Section 2.1, local conditions
218 altering simulation results for the early and latecomers exist [53,71], e.g. the initial positions of individuals, as well as
219 uncertainties in $v_{pref,i}(x, y, t)$ and in path selection. To avoid such behavioural effects, the first 5% and last 5% of arrived
220 evacuees were excluded in evacuation time estimation. To this end, the evacuation times [s] of the individuals' 5th ($T_{e,0.05}$)
221 and 95th ($T_{e,0.95}$) percentile were additionally calculated.

222 The *overall average evacuation curve* represents the number of arrived evacuees $P_e(t)$ during the time (graphical vis-
223 ualization) [67,72]. Average, maximum and minimum evacuation curves were assessed to graphically express the devia-
224 tion within the sample. Moreover, the evacuation curve for each safe area was calculated.

225 The *effective average flow of evacuees arrived in a safe area* F_e [persons/s] describes the swiftness of the evacuation
226 process [73,74]. F_e was calculated as the ratio between the number of arrived individuals ($P_e=5\%$, $P_e=50\%$ and $P_e=95\%$)
227 and the related time difference between $T_{e,0.05}$ and $T_{e,0.50}$ (for $P_e=50\%$; $F_{e,0.50}$) or $T_{e,0.95}$ (for $P_e=95\%$; $F_{e,0.95}$). $F_{e,0.95}$ resumes
228 the overall process swiftness. $F_{e,0.50}$ shows the **median** trend in the evacuation flows, determining the slope of the evacu-
229 ation curve in its central part. These values should be maximized to speed up the evacuation and to increase the safety of
230 individuals (by reducing their exposure to potentially risky floodwaters conditions). The value was evaluated for the
231 whole process and for each safe area.

232 The *number of out-of-time evacuees (including casualties)* P_O [persons] shows how many evacuees cannot reach a
233 gathering area within the simulation time. P_O was also expressed in percentage terms ($P_{O,\%}$ [%]). Moreover, $P_{O,street}$ pro-
234 vides the number of *out-of-time evacuees* for each space (e.g. street) in the outdoor built environment. According to the
235 rules for evacuation stop in the behavioural simulation model (see Section 2.1) [35,68], **it could** be possible to identify
236 the percentages of *out-of-time evacuees* **considering** :

- 237 • *latecomers* by $P_{O,la}$ [%], **which are the** evacuees located near a safe area or in not risky condition at the end
238 of the simulation (i.e. lowest DV levels);
- 239 • *spontaneous gathering evacuees* by $P_{O,sp}$ [%];
- 240 • *casualties* (considering evacuees exposed to $DV > 1.2$ m²/s) by $P_{O,ca}$ [%].

241 Such values were calculated for each street (e.g. $P_{O,ca,street}$) in both absolute and relative terms. *Latecomers*, *spontaneous*
242 *gathering evacuees* and *casualties* were represented on the outdoor built environment layout to graphically show the areas
243 affected by such phenomena. In general terms, P_O should be minimized as long as it is complementary to P_e . In particular,
244 $P_{O,ca}$ should be primarily minimized.

245 The *street crowding* $P_{cr,street}$ [persons] specifies how many evacuees go through a given street in the urban layout while
246 evacuating [57,73,75]. The higher $P_{cr,street}$, the higher the number of individuals who can be exposed to local floodwater
247 conditions and to possible individual-individual interactions (by including queuing phenomena). $P_{cr,street,\%}$ [%] was nor-
248 malized by the maximum $P_{cr,street}$ value within the simulated area.

249 2.2.2 KPIs relating to the built environment

250 The *KPIs relating to the built environment* were calculated for the entire simulation area or for a **single outdoor space**
251 (i.e. a street, a square). They trace the risk level depending on the main behavioural design-based risk factors (i.e. *out-of-*
252 *time evacuees*; *DV* levels; crowding levels), and with respect to the whole simulation time. To support the prioritization
253 of interventions in the built environment, they were also offered via risk maps of the built environment [7,60,76].

254 The complete description of these KPIs is reported in Appendix C. The following dimensionless KPIs were considered:

- 255 • $R_{area,scen}$ [-] and $R_{street,scen}$ [-] respectively assess the conditions of the whole area and of a single outdoor space.
256 They were evaluated considering the following comparable scenarios sets: (a) the same implemented risk
257 reduction solutions and different floodwater events; (b) the same floodwater event and different risk reduction
258 solutions. They define the worst scenarios within the comparable ones and investigate the effectiveness of
259 risk-reduction solutions;
- 260 • R_{street} [-] assesses the risk indices of a given outdoor space in comparison to other streets and squares, by
261 considering a given scenario. In particular, it highlights the riskiest parts of the outdoor built environment
262 under certain hydrodynamic conditions. Thus, it **points out** where risk reduction strategies should be focused.

263 These KPIs were based on three main behavioural design-based factors: (a) the risk for *out-of-time evacuees*, due to
264 the presence of *casualties*, *latecomers* and *spontaneously gathering evacuees* (e.g., for the whole area $R_{O,area,scen}$); (b) the
265 risk due to the floodwater level in the built environment (e.g., for the whole area $R_{DV,area,scen}$); (c) the crowding risk, which
266 considers how many evacuees can move in the built environment or in a street/square into it (e.g., for the whole area
267 $R_{cr,area,scen}$).

268 These risk factors were combined according to the Analytical Hierarchy Process (AHP) methodology [10,77,78], since
269 they do not necessarily have the same relevance. The selected KPIs were pairwise compared in the AHP, **basing on Saaty's**
270 relative importance **scale** (1-equal to 9-extreme). **This procedure allows calculating the** related priority weights, according
271 to the principal eigenvector of the decision matrix in the AHP method. The proposed priority weights were **considered**
272 **acceptable** if the Ratio of Consistency RC associated with the performed pairwise comparison was lower than 10%. The

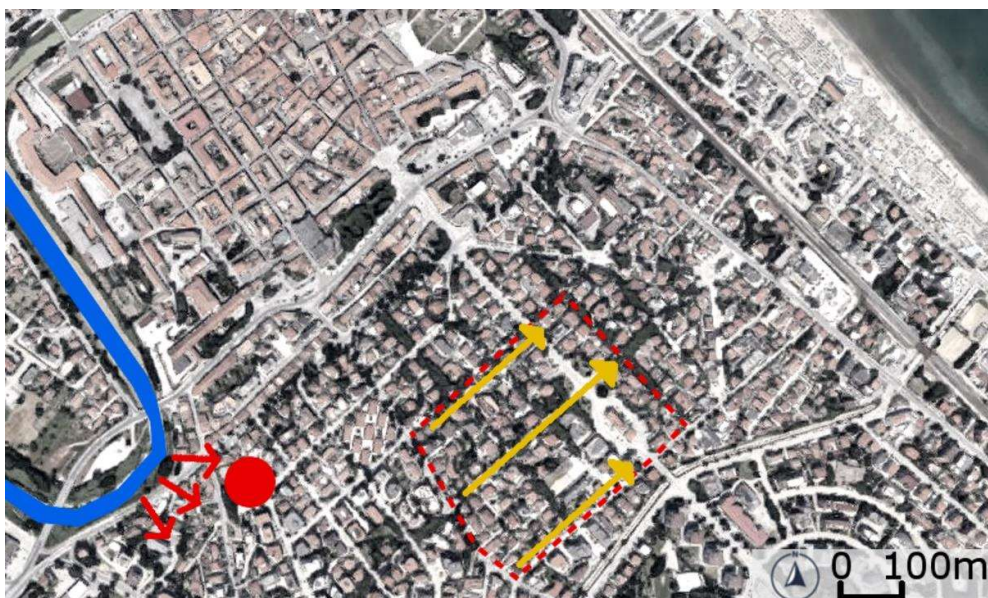
273 lower RC, the more confident the priority weight estimation. As a result of the AHP application, KPIs always range from
274 0 to 1 (which corresponds to the maximum risk). KPIs were based on a two-level Decision Hierarchy. A similar approach
275 was already used in flood risk assessment (e.g. [10]) and also in other kinds of disasters in outdoor built environments
276 (e.g. earthquakes [79]).

277 2.3 Case study definition

278 An area in the city centre of Senigallia (AN, Italy), recently affected by floods, was chosen as a case study. Senigallia
279 is located along the Adriatic coastline and built on a floodplain, near the estuary of the Misa River. Moreover, it has a
280 compact urban fabric, characterized by scarcely permeable surfaces and narrow streets. As a consequence, the water
281 spreading during floods flows like in an open compound channel.

282 Figure 1 shows the location of the area (red dashed rectangle) in the urban fabric. Figure 1 also graphically shows: the
283 main streets along the upstream-downstream direction (yellow arrows); a portion of the Misa River (in blue), which is the
284 flood source; the Anna Frank gardens (red circle), discussed in the following as source locations of the used boundary
285 conditions. This area was chosen because of the relevant inundation that occurred in May 2014, especially affecting the
286 main central street in the built environment (A. Garibaldi street, in Figure 2-A) and the upstream part of the domain. The
287 choice of such a scenario (which is representative of the urban built environment as discussed above) also allowed easily
288 retrieving input data on geometrical, hydrodynamics and exposed people, since it was investigated in previous works (e.g.
289 [17,80]).

290



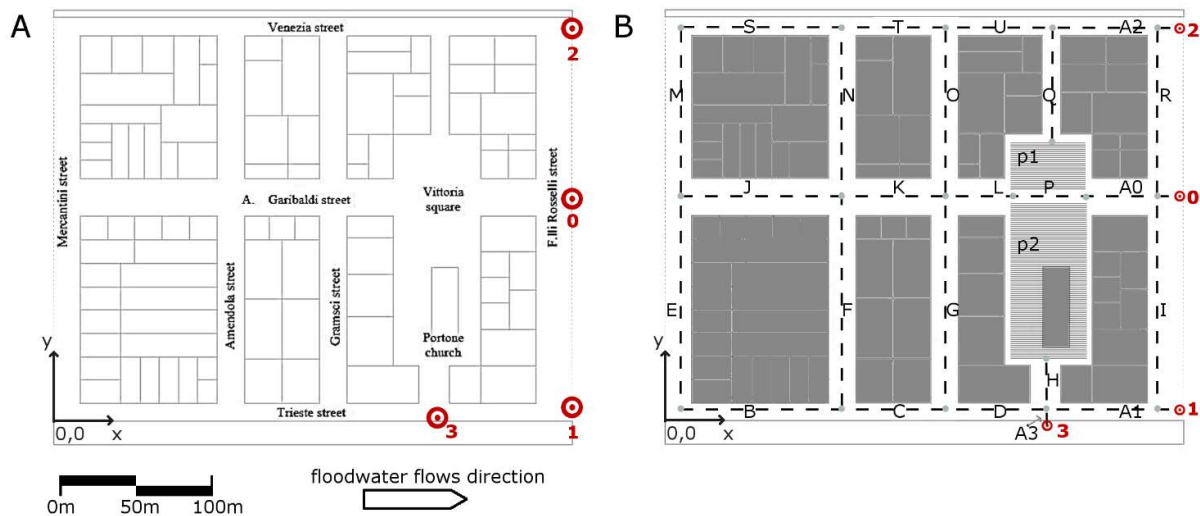
291

292 **Figure 1.** Overview of the case-study area: domain limits (red dashed perimeter); main upstream-downstream streets (yellow arrows);
 293 the Misa river as the source of the flood (blue line and red arrows); the place where data were collected during the 2014 flood (red
 294 circle, *Anna Frank* gardens). Adapted from Google Maps, last access: 20/10/2019.

295

296 The geometrical layout of the urban scenario (also used in FlooPEDS preliminary tests [17]) was divided into a series
 297 of rectangular **subdomains**. In each subdomain, floodwaters conditions could be taken as homogeneous, according to the
 298 solver structured grid with spatial resolution of $(\Delta x, \Delta y) = (0.8, 0.5)\text{m}$. Figure 2 traces the domain, having an area of about
 299 $90,000\text{ m}^2$ ($x = [0, 350]\text{m}$; $y = [0, 265]\text{m}$). Figure 2-B also shows the division of the outdoor built environment into streets
 300 (dashed lines) and squares (hatched rectangles), and the position of the safe areas. Comparing Figure 2-A and Figure 2-
 301 B, the three main streets along the upstream-downstream direction (yellow lines in Figure 1) are: A. Garibaldi street as
 302 the outdoor spaces (i.e. streets) J, K and L, Trieste street as B, C, D, A1; Venezia street as S, T, U, A2.

303



304

305 **Figure 2.** Simplified domain modelling: (a) a general overview of the simulation area limits (dashed light grey lines) by including
 306 domain origin, metric scale, floodwater flows main direction (arrow on the bottom), place names and safe areas with the related identi-
 307 fication number (red circles); (b) streets (dashed lines connecting two grey circles) and squares (hatched areas) with related identifi-
 308 cation codes, and buildings (grey blocks).

309

310 Two *flood scenarios* were simulated: (1) levee-failure (Section 2.3.1) and (2) river-overflow (Section 2.3.2). The latter
 311 case was based on existing data and statistics, although extreme and precautionary assumptions were made. The hydro-
 312 dynamic conditions were imposed at the upstream boundary and linearly varied between each of the steps according to

313 the specific assumptions (see D and V reported in Table 1 and Table 2). A reflecting condition was imposed both laterally
314 and at the downstream boundary.

315 The input data about the evacuation scenario are described in Section 2.3.3. Finally, KPIs application for scenarios
316 comparison is described in Section 2.3.4.

317 2.3.1 Levee-failure scenario

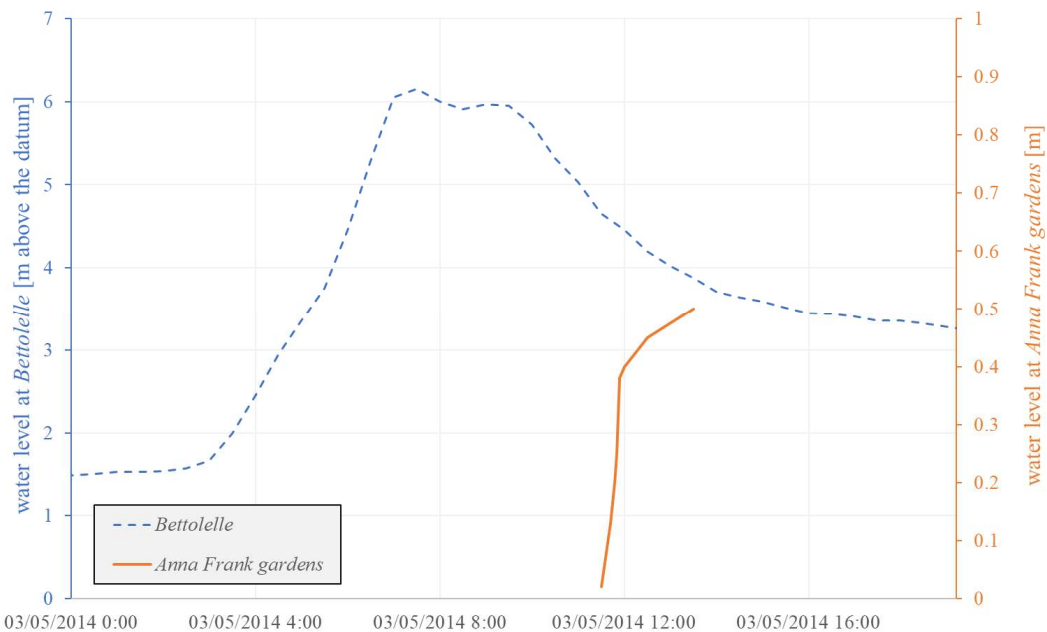
318 Information on the levee-failure was collected from analyses on the actual flood features (water depth D and speed V)
319 observed during the event in the case study area. The event time series were reconstructed from videos recorded during
320 the 2014 flood in the *Anna Frank* gardens (red-circled area in Figure 1, located close to both river and study area). A
321 reduced distance (about 300m) exists between such location and the west boundary of the numerical domain. Thus, hy-
322 drodynamic simulations used these recorded time series. Input data concerning D and V recorded on May 3rd, 2014 from
323 11.30 am to 1.30 pm (see Table 1) were assigned as upstream boundary conditions. Figure 3 shows the hydrograph
324 referring to the most downstream available water level measurements (the hydrometer is located at *Bettolelle* station,
325 which is about 7 km far from the case-study area).

326

327 **Table 1** Levee-failure input data used as boundary conditions (at $y=0$ in Figure 2) for the hydrodynamic simulations

t [s]	D [m]	V [m/s]
0	0.02	0.06
720	0.13	0.31
1080	0.20	0.45
1200	0.25	0.57
1440	0.38	0.85
1800	0.40	0.90
3600	0.45	1.01
7200	0.50	1.12

328



329

330 **Figure 3.** Water level evolution during the May 2014 flood: hydrograph (dashed line) recorded at *Bettolelle* station; water level chosen as the boundary condition in the case-study domain (solid line), reconstructed using the data recorded at the *Anna Frank gardens*
 331 (see red circle in Figure 1; data are offered by Table 1).
 332

333 2.3.2 River-overflow scenario

334 We assumed that an overflow hazard might characterize a river stretch close to the city centre (see Figure 1) where:
 335 (a) the cross-section significantly reduces up to a width smaller than 20m, depending on the flow condition; and (b) the
 336 flow reaches the bank almost perpendicularly.

337 Boundary conditions were based on analyses aimed at identifying the return period of the Misa River discharge. Depending on the method applied for such estimate⁴, the mean discharge ranges between 400 and 600 m³/s for return periods
 338 $T_R=(100-500)$ years (e.g., [80]), while the maximum discharge ranges between 300 and 900 m³/s for $T_R=(50-200)$ years.
 339 Under the worst-case scenarios, the highest water level can be assumed for this reach of the river (e.g. about 2m over the
 340 right bank over which overflow is assumed to occur). Such assumption is consistent with: 1) the features of the left bank,
 341 which is some meters higher than the right bank; 2) a discharge related to a large return period, i.e. of the order of 900
 342

⁴ *Autorità di Bacino Regione Marche, Delibera C.I. n. 67/2016, Elaborato "A"*; website: http://www.regione.marche.it/Portals/0/Paesaggio_Territorio_Urbanistica/AdB/PAIMarche/DelComIst/allegati/del160325_67_ElaboratoA.pdf. Hydrological and hydraulic report for the construction of the hydropower plant "Bettolelle" in the Misa River; website: <http://www.ambiente.marche.it/Portals/0/Ambiente/Pubblicazioni/V00508/6fb572e4-92eb-4ba3-b225-314fb2f15852.pdf> (last access 21/11/2019)

343 m³/s. It was thus assumed that the water overflows through a bank length $b=(110\div 120)$ m, with a head over the bank
 344 $h_l=2$ m, which was taken as constant along b . As a consequence, the geometry of the bank was provided as almost rectan-
 345 gular. The water discharge Q flowing down from the bank was estimated using the typical law applied to broad-crested
 346 weirs. Q was assumed as proportional to both b and $h_l^{3/2}$ as in Equation 12:

$$348 \quad Q = 1.7C_d b \left(h_l + \frac{v_l^2}{2g} \right)^{3/2} \quad (12)$$

349
 350 where v_l is the flow velocity and C_d is the discharge coefficient. A suitable choice of the involved terms (e.g., $v_l \sim 5$ m/s
 351 during flood conditions, $C_d \sim 0.6$) leads to a discharge equal to about 700m³/s.

352 Finally, the overflowing discharge was completely transferred to the study area (about 600m far from the overflow
 353 location), i.e. neglecting dissipation and water infiltration. Although strong, such an assumption represents an ideal ex-
 354 treme condition. It allows properly understanding the benefits of risk reduction strategies when the flood condition is
 355 significantly different from the levee-failure one.

356 The overflow phenomenon can be thought significantly rapid along the rising limb of the hydrograph. Table 2 reports
 357 the selected input data (D , v) and the assumed discharge Q at each stage. Depending on the water depth at the upstream
 358 boundary ($D=1.1$ m) and domain width (265 m along the y -direction), the velocity modulus varies between 2.30 and
 359 2.40 m/s.

360

361 **Table 2** River-overflow input data used as boundary conditions (at $y=0$ in Figure 2-A) for the hydrodynamic simulations

t [s]	Q [m ³ /s]	D [m]	v [m/s]
0	670	1.10	2.30
50	685	1.10	2.35
600	700	1.10	2.40

362

363 2.3.3 Evacuation simulation setup for the case study

364 Each evacuation simulation involved 300 individuals to represent the number of individuals located in adjacent
 365 buildings. In particular, for each building, the building surface [m²] and the intended use (i.e.: residential, commercial,
 366 other public buildings) were assessed through an infield survey. Then, the following occupant load values were applied

367 with respect to each intended use according to the Italian Fire Safety Code [81]: residential, 0.05pp/m²; commercial, 0.4
368 pp/m²; other public buildings, 0.7pp/m². This process allowed calculating the possible occupant capacity for each
369 building. According to a conservative approach, individuals were considered as located outdoor (i.e. near the building
370 access) and not able to enter the nearest building and move vertically.

371 When the evacuation started, individuals tried to move towards the safe areas according to the modelling criteria (see
372 Section 2.1 and Appendix A). Safe areas were characterized by ground elevations and were placed at the downstream
373 area exits, as described in [17,18]. They are shown in Figure 2 and represent the evacuation target for the evacuees.

374 2.3.4 KPIs application for scenarios comparison

375 KPIs defined in Section 2.2 were firstly applied to derive the outdoor built environment safety in the pre-strategies
376 proposal scenario (in the following, the “*original scenario*”). The most critical floodwater conditions between the ana-
377 lyzed flood scenarios (levee-failure and river-overflow) were retrieved. The outcoming flood scenario was considered for
378 the proposal of risk reduction strategies. Finally, such strategies were implemented within the outdoor built environment
379 and their effectiveness was evaluated by comparing KPIs. Equation 11 shows the percentage difference $dKPI_{red-pre}$ [%] of
380 a given KPI by considering the *original scenario* (KPI_{pre}) in respect to the one with risk reduction strategies (KPI_{red}) [57]:

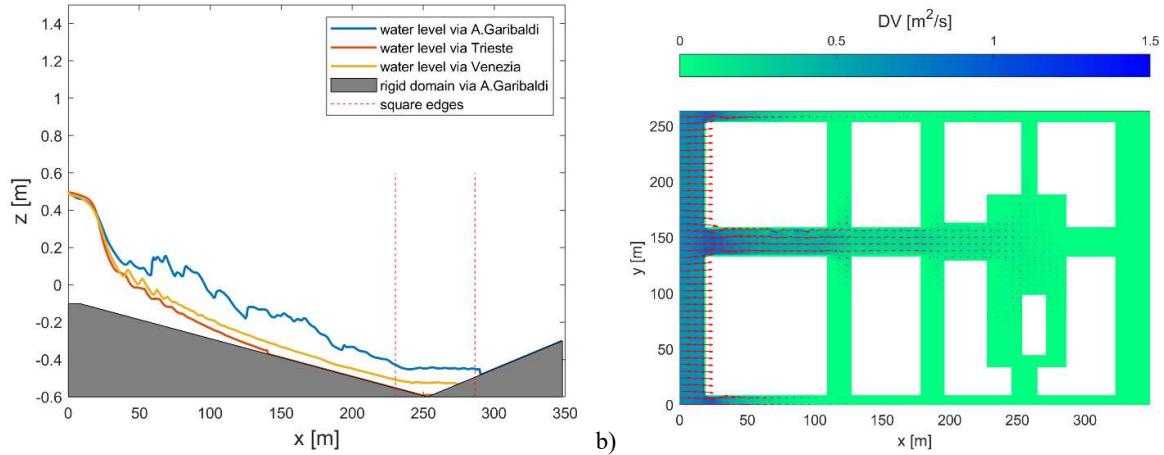
$$381 \quad dKPI_{red-pre} = \frac{KPI_{red} - KPI_{pre}}{KPI_{pre}} \cdot 100[\%] \quad (11)$$

382 For risk indices $R_{area,scen}$ and $R_{street,scen}$, negative $dKPI_{red-pre}$ values imply a reduction of the risk levels.

383 3 Results

384 3.1 Flood scenarios

385 Figure 4 shows the hydrodynamic outputs for the levee-failure scenario. In this scenario, the maximum discharge (peak
386 condition) occurs after 7200s. Both panels of Figure 4 refer to this moment in hydrodynamic simulation results. Figure
387 4-A shows the streamwise evolution of the water-surface profile along the West-East streets of the analysed domain
388 (yellow lines in Figure 1). Figure 4-B illustrates the top view of the DV map overlapped to the numerical domain.



389

a)

b)

390 **Figure 4.** Hydrodynamic results of the levee-failure simulation after 7200s (peak condition): a) streamwise sections; b) DV map (red
 391 arrows are the speed vectors; buildings-obstacles are the white areas).

392

393 In more details, the flow depth is higher along the streets J, K, L, A0 (blue line in Figure 4-A) than along the other two
 394 parallel streets, that are streets B, C, D, A1 (red line) and streets S, T, U, A2 (yellow line). The colour map shown in
 395 Figure 4-B confirms this result: larger values of DV are met along streets J, K, L, A0 (see the lighter colours at $y \sim 150$ m
 396 and darker colours at $y \sim 1$ m and $y \sim 256$ m). Concerning the crossing streets, the leftmost one is characterized by the largest
 397 flow, as it is the closest to the source/boundary condition, with the water level being the highest ($z=0.5$ m) and DV reaching
 398 the maximum value of $0.8 \text{ m}^2/\text{s}$. Conversely, DV becomes nearly zero downstream, i.e. within the square area located
 399 around $x = 260$ m (square P-p1-p2, indicated by red vertical lines in Figure 4-A).

400

The speed vectors in Figure 4-B shows the main circulation patterns generated within the domain. The speed reduces
 401 while moving downstream. Moreover, the water flow entering the crossflow streets ($x \sim 115$ m, $x \sim 190$ m) is visible as bend-
 402 ing arrows (see also the little perturbations in the water-surface level in Figure 4-A).

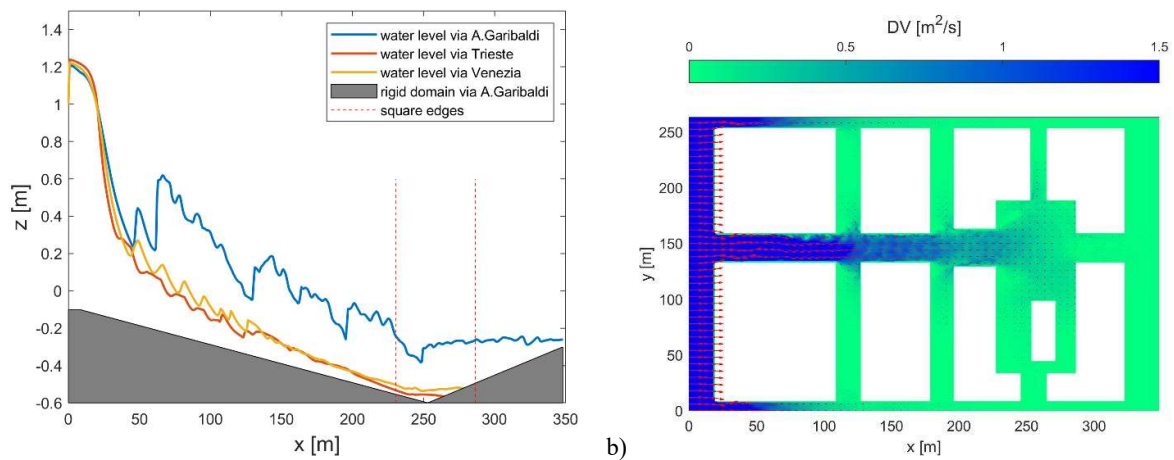
403

Figure 5 shows the outputs of the river-overflow tested scenario. In this scenario, the maximum discharge (peak con-
 404 dition) occurs after 600s. Both panels of Figure 5 refer to this moment in hydrodynamic simulation results. Figure 5-A
 405 shows the streamwise section and the water-level profiles relevant to the central section of the streamwise streets. The
 406 two lateral streets are illustrated in red (streets B, C, D, A1) and yellow (streets S, T, U, A2), while streets J, K, L, A0 are
 407 plotted in blue. As for Figure 4-B, Figure 5-B shows the DV distribution through a colour map. The largest DV values
 408 occur at the upstream boundary, where $DV=1.3 \text{ m}^2/\text{s}$. In contrast to the levee-failure case, high speeds and reduced depths
 409 occur at the intersections between the streets J, K, L, A0 and: (1) the crossflow streets, that are streets F and N, and streets
 410 G and O (also see DV at the intersection at about $(x,y)=(115,150)$ m in Figure 5-B); (2) the square (P-p1-p2). Considering

411 the street intersections, Figure 5-B also shows how speed vectors (red arrows) are not straight but visibly bend towards
 412 the crossflow streets. Furthermore, Figure 5-A shows a large perturbation of the water surface just downstream of the
 413 intersections (e.g., see the blue line at $x \sim 120\text{m}$ and 190m). Such a feature is due to both large flow intensity and rapid
 414 friction reduction at the intersections. **In particular, the friction** changes from a relatively large value (due to both bottom
 415 and vertical obstacles/blocks) to a much smaller value (due to the only bottom contribution).

416 **Given** the above, the river-overflow scenario is significantly more severe than the levee-failure scenario, considering
 417 that it is based on ideal and largely conservative assumptions.

418



419 a) b)
 420 **Figure 5.** Hydrodynamic results of the river-overflow simulation after 600s (peak condition): a) streamwise section; b) DV map.

421

422 Hydrodynamic results provided useful insights for the following behavioural simulations. **It** is observed that the levee-
 423 failure case reaches almost steady conditions after 600s, while steadiness is reached after 300s in the river-overflow case.
 424 Thus, the total time of behavioural simulations is respectively assumed equal to 600s and 300s.

425 3.2 Original scenario: simulation results

426 Table 3 offers the simulation results concerning the evacuation process for the two considered scenarios. The number
 427 of arrived evacuees, the related evacuation times and the evacuation flows are compared. Figure 6 represents the related
 428 evacuation curves. The two flood scenarios are characterized by significant similarities about: (a) the evacuation path
 429 selection; (b) the position of *out-of-time evacuees*.

430 Regarding the path selection, evacuees prefer to move towards the outdoor spaces which are orthogonal to the flood-
 431 water direction in both scenarios (streets F and N, streets G and O; squares p1 and p2; streets I and R). **In fact, the DV**

432 conditions **in these areas** are less critical (Figure 4 and Figure 5). As shown by Figure 4, this phenomenon is more relevant
433 in river-overflow, because DV values are generally higher in comparison to the levee-failure scenario. This evacuees'
434 choice affects the use of the safe areas. As shown by Table 3, the safe area 0 seems to be the less used one in both
435 conditions, because it is placed in the main floodwater flow direction. Nevertheless, about half of the evacuees **can** gain
436 a safe area within the simulation time in both cases. In fact, according to Table 3, P_e is similar for both the flood scenarios
437 (percentage difference of about 6% on the average values).

438 About data on the *out-of-time evacuees*, Table 4 outlines areas and causes that prevent them from reaching a safe area
439 within the simulation time. In general terms, at the end of the evacuation, **most out-of-time evacuees are located along the**
440 streets E and M, streets F and N, streets G and O, and the upstream part of streets J and K. Figure 7 summarizes the
441 positions of *out-of-time evacuees*. In both cases, evacuees located downstream are latecomers influenced by:

- 442 • their initial position, far from the selected safe area;
- 443 • floodwater **interactions** because M values along the chosen paths decrease their speed.

444 When the simulation ends, most of these evacuees are located in the crossflow streets immediately downstream in the
445 domain. In fact, they remain close to buildings because of attractive forces [17] and because DV levels are lower than in
446 the main streets, which are parallel to the main floodwater flow.

447 Differences in the evacuation results in each flood scenario are affected by “how” the floodwater events specifically
448 develop during the simulation time depending on the hydrodynamic conditions themselves. In the river-overflow scenario,
449 DV values quickly increase during the first part of evacuation time, by immediately reaching critical conditions for indi-
450 viduals' stability. As a result, a significant number of *out-of-time evacuees* (42%) are influenced by critical DV conditions,
451 thus provoking casualties (compare to Figure 7-B), too. On the contrary, in the levee-failure scenario, the stability thresh-
452 old is not reached in the simulation domain, by provoking no casualty.

453 Additional differences are related to “how” the evacuation process develops over time. The overall evacuation curves
454 in **both scenarios** share the same sigmoidal function trend (compare to Figure 6). However, the evacuation process in the
455 levee-failure scenario seems to be faster than the one in river-overflow, especially in the first part of the evacuation. In
456 fact, according to Table 3, $F_{e,0.50}$ for the levee-failure is at least more than 3 times greater than the one in the river-
457 overflow. Such a result is graphically shown by the slope of the overall average evacuation curves, **which is** higher for
458 the river-overflow scenario, **as shown in Figure 6-B**. This output is essentially due to the lower DV level in levee-failure
459 when compared to **the one observed** in the river-overflow (compare to Section **Error! Reference source not found.**
460 results). Levee-failure scenario implies lower importance of individual-floodwaters interactions while moving (i.e. higher
461 evacuation speeds; lower possibility to stop moving because of critical DV levels). Thus, most evacuees can reach a safe

462 area within the first 100s in the evacuation simulation. When the evacuation time increases ($>100s$), the levee-failure
 463 scenario is mainly characterized by the arrival of *latecomers*. In fact, evacuees can still move in the considered area, but
 464 they are slowed down by the *DV* levels. Figure 6 shows a significant asymptotic trend in the evacuation curve essentially
 465 due to such a phenomenon. Meanwhile, $T_{e,0.95}$ for the levee-failure scenario increases and the final overall $F_{e,0.95}$ proves
 466 to be fairly lower than the one for the river-overflow scenario. The same trend can be noticed for each of the safe areas.
 467 It is worthy to notice that safe area 3 is more affected than the others by the critical *DV* levels noticed in the upstream part
 468 of the urban scenario, as shown, for instance, by $F_{e,0.50}$ in the levee-failure scenario.

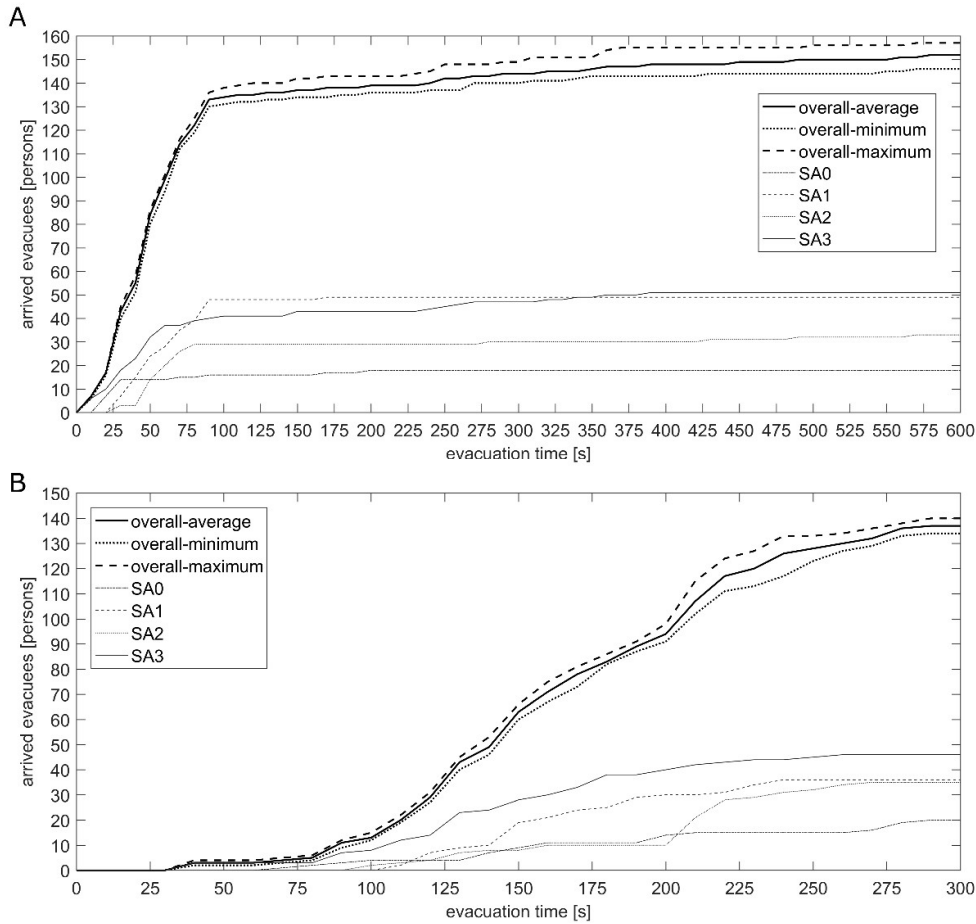
469 Finally, during the evacuation process, several evacuees change their initial evacuation target, which is the nearest safe
 470 area. They can change their target because of [17]: (a) group motion criteria; (b) surrounding critical *DV* levels retrieved
 471 along the path initially selected. The percentage of evacuees changing their initial target in respect of the total number of
 472 arrived evacuees is equal to 34% for the river-overflow and 39% for the levee-failure scenario (see the supplementary
 473 material: S1). In both cases, evacuees' target selection for safe area 1 is essentially affected by the spatial proximity of
 474 safe area 0 and safe area 3. No significant differences are noticed for the other safe areas.

475

476 **Table 3.** Simulation results for levee-failure and river-overflow scenarios, in the original scenario, according to Section 2.2.1
 477 KPIs. Safe areas positions are shown in Figure 2.

Scenario (max sim. time [s])	Reference safe areas	P_e (st. dev.) [persons]	$P_e\%$ (st. dev.) [%]	$T_{e,0.05}$ [s]	$T_{e,0.50}$ [s]	$T_{e,0.95}$ [s]	$F_{e,0.50}$ [persons/s]	$F_{e,0.95}$ [persons/s]
<i>levee-failure (600s)</i>	all	152 (4)	51 (3)	10	46	377	1.71	0.39
	safe area 0	18 (3)	6 (19)	10	22	113	0.45	0.17
	safe area 1	49 (2)	16 (5)	24	56	86	0.44	0.59
	safe area 2	33 (3)	11 (8)	28	58	479	0.29	0.07
	safe area 3	51 (3)	17 (6)	9	42	301	0.60	0.17
<i>river-overflow (300s)</i>	all	137 (2)	46 (2)	85	159	265	0.50	0.44
	safe area 0	20 (1)	15 (1)	73	158	279	0.06	0.07
	safe area 1	36 (2)	26 (2)	111	151	230	0.13	0.15
	safe area 2	35 (2)	26 (1)	108	208	251	0.08	0.13
	safe area 3	46 (2)	33 (1)	45	126	237	0.16	0.18

478



479

480 **Figure 6.** Evacuation curves for the original scenario in case of: a) levee-failure; b) river-overflow. Evacuation curves are offered for
 481 the whole process (including minimum and maximum curves) and for each safe area.

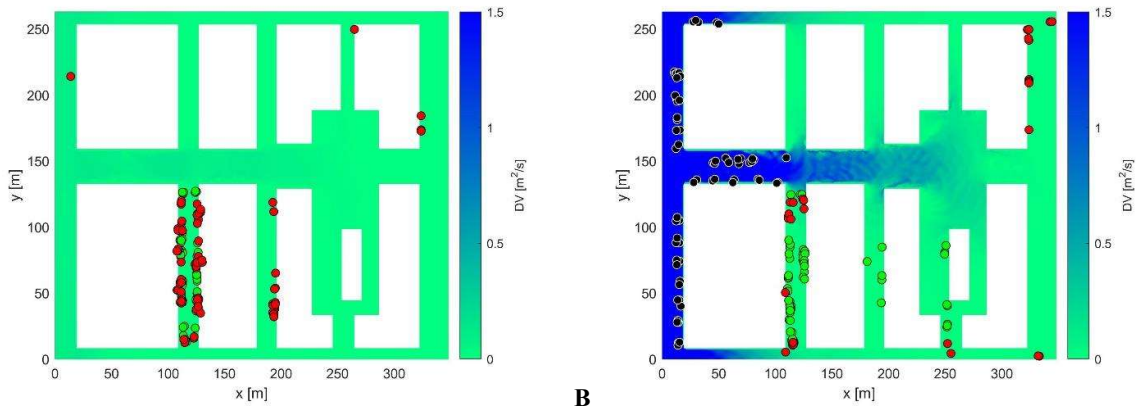
482

483 **Table 4.** Out-of-time evacuees P_O (and their characterization) in the levee-failure and river-overflow simulations, for the original
 484 scenario, according to the KPIs in Section 2.2.1. Percentage values are calculated for the main or secondary related conditions.

Main condition	Secondary conditions	P_O (st. dev.)[per- sons]		$P_{O,\%}$ (st. dev.) [%]		$P_{O,la} - P_{O,sp} - P_{O,ca}$ [%]	
		Levee- failure (600s)	River- overflow (300s)	Levee- failure (600s)	River- overflow (300s)	Levee- failure (600s)	River- overflow (300s)
		all	148 (4)	163 (2)	49 (3)	54 (1)	55-45-0
evacuees who stop upstream (streets E		2 (1)	53 (1)	2 (1)	32 (1)	100-0-0	0-0-100

and M) because of floodwater conditions (e.g. stability loss)							
total number of evacuees located downstream		146 (3)	110 (2)	98 (1)	68 (1)	54-46-0	33-54-13
	evacuees who stop in the main street (streets K, L, A0)	5 (3)	18 (3)	3 (2)	11 (2)	0-100-0	0-18-82
	evacuees who stop near safe area 3	0 (0)	10 (5)	0 (0)	6 (3)	0-0-0	100-0-0
	evacuees who stop near a downstream safe area	4 (2)	12 (2)	2 (1)	8 (1)	100-0-0	100-0-0
	evacuees who stop in the square (square P-p1-p2)	8 (1)	14 (1)	0 (0)	0 (0)	0-0-0	38-62-0

485



486

A

B

487

Figure 7. Position of out-of-time evacuees at the end of the behavioural simulations in case of: a) levee-failure; b) river-overflow.

488

Latecomers (red circles), spontaneously gathering evacuees (green circles), casualties (black circles) are shown on the DV map.

489

490

$R_{area,scen}$ in Table 5 and $R_{street,scen}$ in Figure 7 confirm that the river-overflow leads to a worse outcome. **In this scenario,**

491

the higher impact is due to the floodwater conditions (see $R_{DV,area,scen}$ in Table 5), which increase the number of *out-of-*

492

time evacuees (see $R_{O,area,scen}$ in Table 5) and *casualties* (see $R_{street,scen}$ in Figure 7). On the contrary, crowding conditions

493 (see $R_{cr,street,scen}$ in Table 5) are higher for the levee-failure scenario since the lower DV levels reduce the number of *casu-*
 494 *alties* and allow evacuees to effectively move in the outdoor built environment.

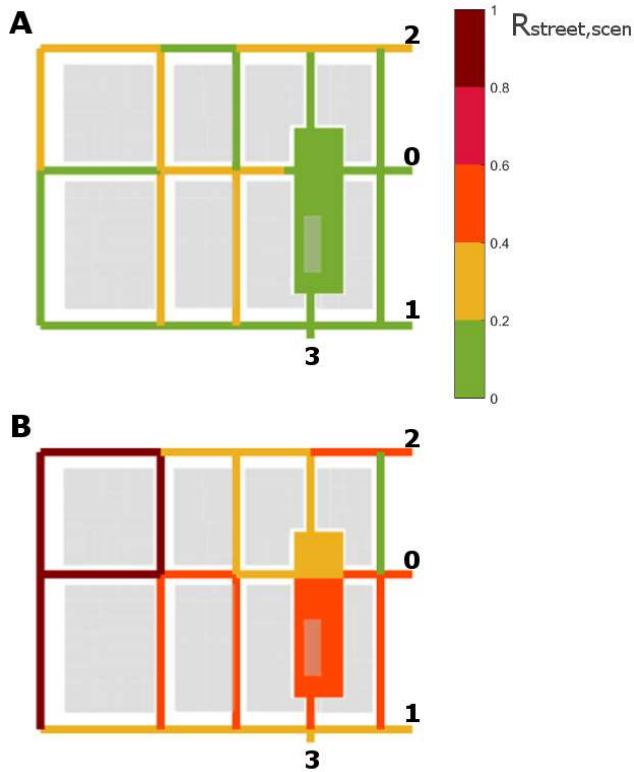
495 Figure 8 summarizes the risk of each outdoor space in the scenario by comparing the river-overflow and the levee-
 496 failure scenario. Raw data are reported in the tables of supplementary material: S2. In both cases, higher risk levels are
 497 reached at the upstream streets (E, J, M, N in Figure 2), mainly because of large DV values and of a high number of *out-*
 498 *of-time evacuees* (essentially, casualties). Streets F, G and N have medium-high $R_{street,scen}$ values for the other streets
 499 orthogonal to the floodwater direction. This effect is due to their related number of *latecomers* and of *spontaneously*
 500 *gathering evacuees* **thanking** the limited DV levels (compare to Figure 7). This phenomenon is more important in the
 501 river-overflow scenario. Finally, some parts of the outdoor built environment placed downstream (e.g. A0, A2, H, I, p2,
 502 R) are mainly affected by higher crowding levels and so their risk is comparable to the ones of streets F and G, especially
 503 in the river-overflow scenario.

504

505 **Table 5** Risk index for the whole area ($R_{area,scen}$) and the related influencing factors, by comparing river-overflow and levee-fail-
 506 ure scenarios.

Scenario	$RO_{area,scen}$	$RDV_{area,scen}$	$R_{cr,area,scen}$	$R_{area,scen}$
Levee-failure	0.27	0.21	1.00	0.30
River-overflow	0.87	1.00	0.81	0.91

507



508

509 **Figure 8.** $R_{street,scen}$ for: a) levee-failure; b) river-overflow. Buildings (light grey blocks) and safe area codes are supplied. The KPI scale
 510 is shown by the color map (0.2 ranges discretization). Raw data are shown by supplementary material: S2.

511 3.3 Risk reduction strategies proposal

512 In the *original scenario*, the percentage of evacuees reaching a safe area is almost the same for both river-overflow
 513 and levee-failure. Nevertheless, the results of Section 3.2 underline how the riskiest scenario is represented by the river-
 514 overflow one because of the critical conditions due to *DV* levels leading to a higher number of *out-of-time evacuees* and
 515 *casualties*. Thus, this flood scenario is considered in the following to propose risk reduction strategies.

516 Figure 9 summarizes R_{street} in the river-overflow scenario (raw data are offered by supplementary material: S3) and
 517 highlights riskier areas, this suggesting practical solutions to support evacuees during hazardous phases.

518 The riskiest streets are located upstream, essentially because of the number of *out-of-time evacuees* (i.e. streets E, J,
 519 M). In such outdoor spaces, most of the evacuees stop moving because they can lose their stability because of floodwaters
 520 conditions. Direct support against the critical *DV* levels should be provided to the individuals located along streets E and
 521 M, to lead them moving towards streets S, J and B or staying here in safe conditions. Evacuees moving along street J
 522 should be **similarly** supported. In addition, the upstream streets that are orthogonal to the floodwater direction (i.e. streets

523 F and G) are riskier than the others because of the number of *latecomers* and *spontaneously gathering evacuees* here
524 thanks to the limited *DV* levels. The evacuees who stop moving here should maintain a safe position while waiting for
525 the rescuers' arrival.

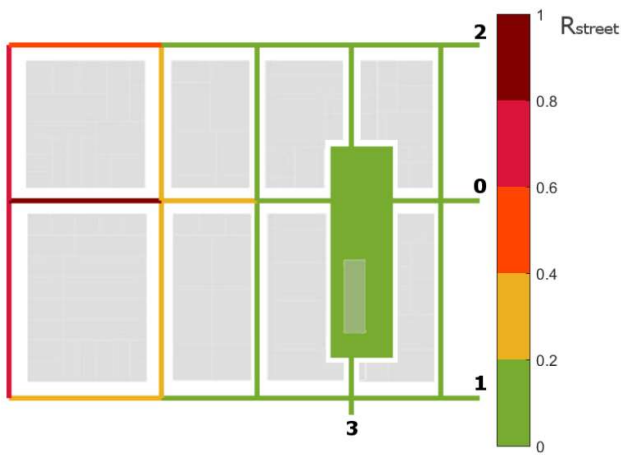
526 Finally, despite the higher crowding level, streets placed downstream are characterized by a negligible risk level in
527 respect to $R_{O,street}$ and $R_{DV,street}$ (that are essentially null and void).

528 In view of the above, two different risk reduction solutions can be provided:

- 529 • the implementation of handrails **can essentially support** evacuees while moving or facing severe *DV* levels
530 conditions (see Section 3.3.1);
- 531 • the implementation of handrails plus raised platforms/sidewalks **can** “separate” the evacuees from the critical
532 floodwater levels, and let them waiting for the rescuers' arrival in safe conditions (see Section 3.3.2).

533 Thus, two related *risk reduction scenarios* are defined and described as follows, while their implementation layout is
534 offered in Figure 10. **In addition to the aforementioned solutions**, signs could be installed in the riskiest areas to inform
535 people about the possible threads (e.g. in terms of possible flood depth) during the normal use of the outdoor built envi-
536 ronment [27].

537



538

539 **Figure 9.** R_{street} representation by considering the river-overflow conditions in the original scenario. Light grey blocks are the buildings,
540 while safe area codes are supplied. The KPI scale is shown by the colour map involving a 0.2 ranges discretization.

541



542

543 **Figure 10.** Proposed risk reduction strategies and their positioning in the related scenarios: a) handrails implementation (dashed lines);
 544 b) handrails+raised platforms (rectangles, to qualitatively represent their areas; identification codes defined as in Table 6). Safe areas
 545 are pointed out.

546 3.3.1 Strategies proposal: handrails implementation

547 Handrails are placed along the sidewalks. They help evacuees maintaining stability while moving towards a safe area
 548 [17,21,37]. In most cases, this solution maintains a low impact on the existing built environment because the handrails
 549 could be implemented on the existing fences or building walls.

550 In the related simulations, we assumed that evacuees supported by handrails could not lose their stability but they could
 551 not also increase their speed (conservative approach in respect to the total evacuation time) [21,35,37,44,45]. This as-
 552 sumption was contemplated in some modelling approaches concerning flooded environments [17,46,47] and it can be
 553 considered valid within the floodwater conditions provided by the simulations ($D(x,y,t) < 1.2\text{m/s}$ and $V(x,y,t) < 3.2\text{m/s}$) [38].

554 Handrails are hence placed at the street boundaries (building walls, fences), where floodwater speeds are reduced due
 555 to the no-slip condition at the wall. Safe areas positions and identification codes are the same as in the *original scenario*.

556 Figure 10-A shows that handrails are mainly placed along upstream streets (i.e. streets B, E, J, M, S) because of their
 557 critical DV levels. Meanwhile, evacuees moving along the other downstream street (e.g. N and F) could be limitedly
 558 supported by handrails because no stability loss phenomena are detected in the river-overflow scenario. Anyway, hand-
 559 rails could be implemented in a widespread manner into the outdoor built environment to support evacuees in other
 560 floodwater conditions with higher DV levels.

561 **3.3.2 Strategies proposal: handrails+raised platform implementation**

562 Raised platforms or sidewalks should be easily reached by the evacuees so as to wait for rescuers in safe conditions,
563 thus being considered safe areas. Thus, in this scenario, we assumed that the position of these elements **was** associated
564 with additional safe areas in the outdoor layout. **Each platform** should be also **marked** by clear and visible (in terms of
565 legibility and aesthetics) identification signs, which could inform the community about the use of the areas also in non-
566 disaster conditions (to be seen by both residents and visitors) [27].

567 These platforms are placed along upstream streets (i.e. streets E, J, M) and in the main layout areas where *spontane-*
568 *ously gathering evacuees* are noticed (i.e. streets F and N), according to the simulation results of the original scenario (see
569 Figure 7). Thus, nine safe areas are proposed by: (a) maintaining safe areas 1, 2 and 3 and removing safe area 0 (which is
570 the less used); (b) introducing six safe areas on raised platforms. Their position is shown **in** Figure 10-B. Anyway, hand-
571 rails are still implemented **along the** streets B, E, M and S to avoid individuals losing their stability because of critical
572 floodwater levels, and so to allow them to reach the raised platform. Table 6 quantitatively describes the raised platforms
573 and their implementation according to the identification codes (as safe areas) in Figure 10-B. **Table 6 also provides** details
574 **concerning:** (a) **the** location; (b) **the** average number of evacuees to be hosted according to **the original** scenario results
575 (compare to, e.g., Figure 7); (c) **the** related minimum wait area; (d) **the** possible width (orthogonal to the street) and length
576 (parallel to the street) of the area; (e) **the** height of the platform from the ground; (f) **additional** notes on the possible
577 implementation in the considered scenario.

578 In particular, each platform dimension (area [m²]) should be great enough to host the average number of gathering
579 individuals (estimated according to P_O values in original scenario simulation) in proper density conditions (3pp/m², to
580 allow them to wait without contact phenomena [82,83]). Their height from the ground should avoid the possibility that
581 floodwaters interfere with evacuees while they are waiting (railings should be always provided). Moreover, their imple-
582 mentation in the outdoor layout should guarantee:

- 583 • adequate access points to ensure the individuals reach the top of the platform (stairs or ramps). In our proposal,
584 the stairs have a tread and a rise of 21cm, while ramps have a slope of 8% to guarantee access by wheelchairs;
- 585 • their overall dimension compatible with the surrounding outdoor layout without consistent modifications to
586 it (i.e. to the exiting sidewalks and car lanes);
- 587 • possible use of the space under the platforms in ordinary conditions.

588 In the following simulations, the two designed raised sidewalks placed along **the street** F are considered as a single
589 safe area because of their proximity in a space with low DV levels.

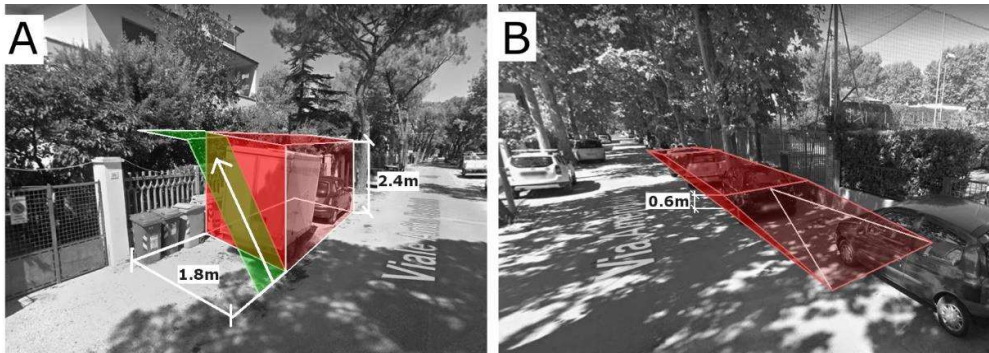
590 Figure 11 shows a couple of possible schematic examples of the raised platform implementation in the case study. In
 591 Figure 11-A a street-level parking lot along the street might be removed to introduce the platform on one street side (view
 592 of scheme for street J – saJ1). The access is guaranteed by stairs while the underlying spaces can be normally used as bus
 593 shelters or waste disposal facilities. In Figure 11-B, a raised sidewalk might be created by removing a couple of street-
 594 level parking lots, accessible by a ramp to guarantee the normal use as a sidewalk (view of scheme for street F - saF).
 595 Similarly, continuously raised sidewalks can be implemented.

596
 597 **Table 6** Data on the raised platforms implementation. Platforms with “*” are split into two equal parts (on each street side), and
 598 the shown dimensions refer to each of the raised sidewalks (thus hosting half of the evacuees’ number).

Street	Safe area code	Evacuees to be hosted	Minimum area [m ²]	Possible width [m]	Possible length [m]	Height from the ground [m]	Notes
E	saE	20	8	1.8	4.5	2.4	removing a street-level parking lot along the street to introduce the platform on one street side; the space under the platform can be normally used as a bus shelter or waste disposal facilities
J	saJ1	10	4	1.8	2.3	2.4	
J	saJ2	10	4	1.8	2.3	2.4	
F	saF*	53	10*	1.8*	5.6*	0.6*	raised sidewalks with removing a couple of street-level parking lots, accessible by a ramp to guarantee the normal use as a sidewalk
M	saM	19	8	3.2	2.4	2.4	raised area within the public square spaces (e.g. garden area)

P	saP	17	6	2.0	3.0	1.0	not currently used vehicle access point; the space under the platform can be normally used as bus shelter or waste disposal facilities
---	-----	----	---	-----	-----	-----	--

599 t



600

601 **Figure 11.** Examples of the possible implementation of raised platforms in the case-study, according to the positions identified by
 602 Table 6: a) removing a street-level parking lot along the street to introduce the platform on one street side, with access by stairs (e.g.
 603 saJ); b) raised sidewalks with access by ramp (e.g. saF).

604

605 **3.4 Effectiveness of the risk reduction strategies**

606 Table 7 offers the simulation results for the river-overflow scenario by considering the *original scenario* versus the
 607 ones concerning the implementation of handrails and handrails+raised platforms. The number of arrived evacuees, the
 608 related evacuation times and the evacuation flows are provided. Figure 12 compares the evacuation curves of these sce-
 609 narios.

610 From a general point of view, according to Figure 12, the overall evacuation curves **concerning** the risk reduction
 611 strategies always demonstrate an improvement in respect to the *original scenario* (also considering maximum and mini-
 612 mum curves). Data and KPIs **are** outlined for the overall simulation area and for each considered safe area. Table 8 shows
 613 data on *out-of-time evacuees*, by including the characterization of the areas and the causes that prevent them from reaching
 614 a safe area within the simulation time.

615 Results of the handrail implementation scenario are quite similar to the ones of the original scenario, both for the
 616 overall evacuation process and for each safe area. The main similarities concern P_e and $F_{e,0.50}$ (see Table 7), the general
 617 evacuation trend (see Figure 12) and the choice of the safe areas (see supplementary material: S4). The effects of handrails

618 are beneficial, especially if considering the possibility to avoid casualties because of body stability loss, as shown by $P_{o,ca}$
619 [%] in Table 8. Nevertheless, the critical floodwater conditions in the upstream streets still slow down the evacuees located
620 in streets B, E, M and S. In fact, some of these individuals can reach a safe area (as shown by increasing P_e in Table 7),
621 but they represent the last arrived evacuees. $T_{e,0.95}$ and $F_{e,0.95}$ slightly increase because of such phenomena. Similarly to
622 the original scenario, 31% of the evacuees change their target because of group motion criteria and surrounding critical
623 DV levels retrieved along the path initially selected. They were too limitedly supported by the handrails while moving.
624 Thus, evacuees still try to spontaneously gather along the street F because of the local beneficial floodwater conditions,
625 as for the original scenario (compare, e.g., with Figure 13).

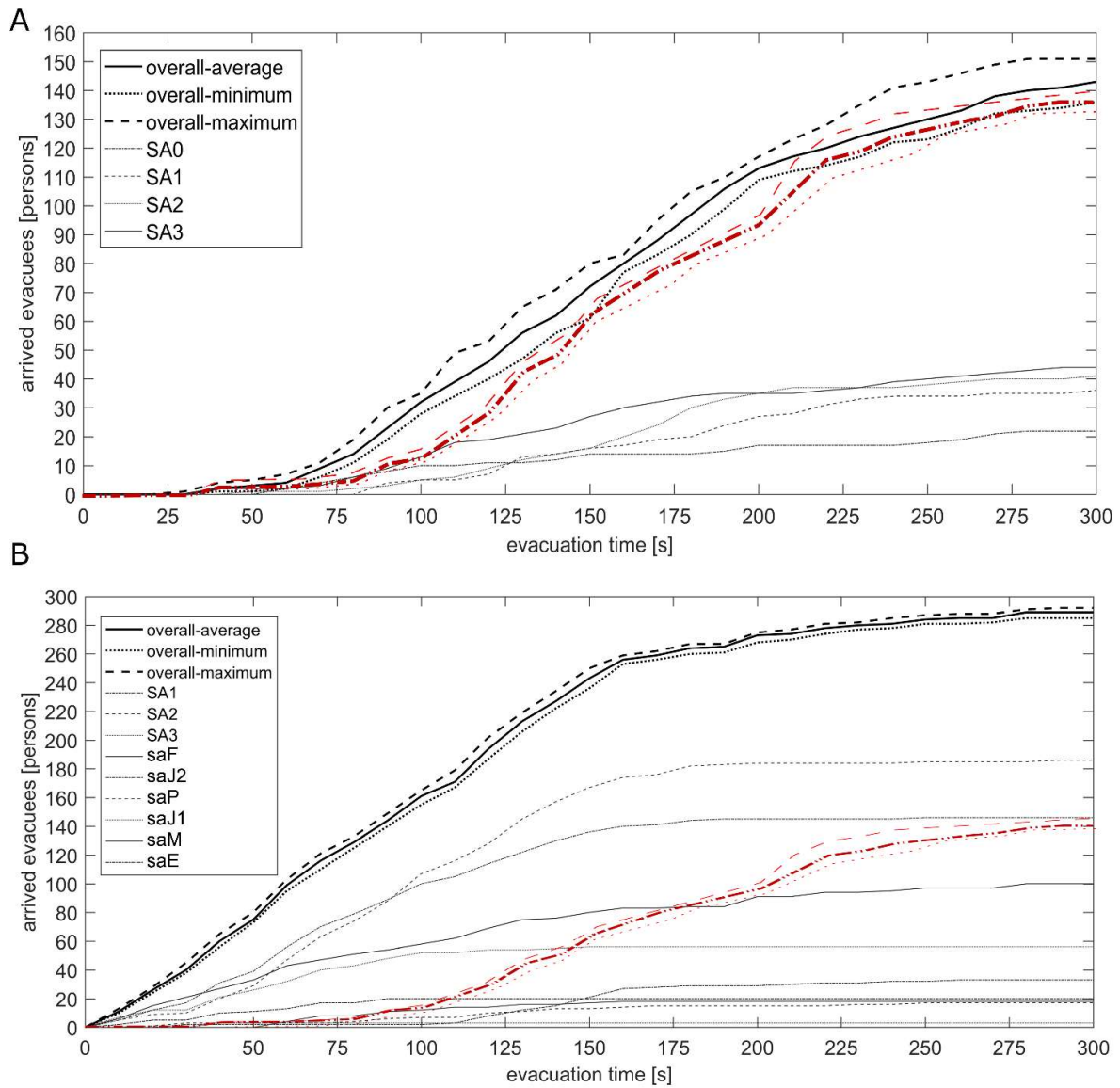
626 On the contrary, the handrails+raised platform implementation significantly decreases the risk conditions for the evac-
627 uees. Firstly, P_e , $F_{e,0.50}$ and $F_{e,0.95}$ increase, as displayed by Table 7. It is worth noticing that the evacuation flows are 3
628 times the ones in the original scenario (see also the slope of the evacuation curves in Figure 12). The combination of
629 handrails in the upstream streets and raised platforms avoids the presence of casualties as well as limits the number of
630 latecomers and *spontaneously gathering evacuees* (see also Figure 13). In fact, the evacuees located upstream can use
631 the handrails to reach the nearest safe areas on the raised platform (i.e. saE, saM, saJ1 and saJ2). According to experi-
632 mental analysis on evacuation behaviours [37], evacuees who cannot reach one of these safe areas prefer to wait near the
633 buildings and spontaneously gather while being supported by the handrails. The time needed to reach the platforms is
634 essentially affected by the floodwater levels and by the distances of the arriving evacuees from the raised platform (see
635 $T_{e,0.95}$ in Table 7).

636 The introduction of raised platforms along the street F and the square P-p1-p2 reduces the number of evacuees arriving
637 at the safe areas placed downstream, and in particular to the safe area 3. In this sense, please also see the supplementary
638 material: S4, i.e. “Difference in arriving evacuees (“initially choosing” minus “reaching”)” data. In fact, evacuees try to
639 minimize their distance from a safe area by using saF and saP. Finally, let comparing the number of evacuees used to
640 evaluate the dimension of the safe areas (according to the *original scenario* simulations, see Table 6) and the number of
641 evacuees who arrived at the raised platforms according to the simulation results (see Table 7). The most significant dif-
642 ferences are retrieved for saF (+86%) and saP (+347%). Anyway, a possible increase of saF and saP surface is still possible
643 in the outdoor built environment. Both sidewalks of street F can be turned into raised elements, while the platform saP
644 can be enlarged since it is placed in a square with gardens.

645

Table 7 Simulation results for river-overflow scenario, in the original scenario and in the ones with risk reduction strategies implemented (handrails; handrails+raised platform), according to Section 2.2.1 KPIs. Safe areas positions are shown in Figure 10.

Scenario (max sim. time [s])	Reference safe areas	P_e (st. dev.) [persons]	$P_e\%$ (st. dev.) [%]	$T_{e,0.05}$ [s]	$T_{e,0.50}$ [s]	$T_{e,0.95}$ [s]	$F_{e,0.50}$ [persons/s]	$F_{e,0.95}$ [persons/s]
<i>Original scenario</i>	all	137 (2)	46 (2)	85	159	265	0.50	0.44
	safe area 0	20 (1)	15 (1)	73	158	279	0.06	0.07
	safe area 1	36 (2)	26 (2)	111	151	230	0.13	0.15
	safe area 2	35 (2)	26 (1)	108	208	251	0.08	0.13
	safe area 3	46 (2)	33 (1)	45	126	237	0.16	0.18
<i>Handrails imple- mentation</i>	all	143 (6)	48 (4)	69	153	270	0.50	0.53
	safe area 0	22 (5)	7 (3)	60	133	259	0.08	0.07
	safe area 1	36 (6)	25 (4)	89	163	253	0.11	0.13
	safe area 2	41 (3)	28 (2)	90	160	246	0.13	0.16
	safe area 3	44 (5)	30 (3)	60	129	258	0.16	0.16
<i>Handrails+raised platform imple- mentation</i>	all	289 (3)	96 (1)	13	91	217	1.60	1.27
	safe area 1	33 (3)	12 (1)	62	143	229	0.31	0.34
	safe area 2	17 (1)	6 (<1)	21	113	194	0.07	0.08
	safe area 3	3 (1)	1 (<1)	33	35	37	0.05	0.06
	saE	20 (1)	7 (<1)	6	40	86	0.25	0.22
	saM	18 (1)	6 (<1)	42	72	138	0.12	0.12
	saJ1	9 (1)	2 (<1)	4	36	90	0.14	0.10
	saJ2	12 (1)	4 (<1)	19	38	67	0.16	0.16
	saF	99 (1)	34 (<1)	10	78	235	0.65	0.40
	saP	76 (2)	27 (1)	50	107	173	0.36	0.42



649

650 **Figure 12.** Evacuation curves for the whole process and for each safe area in the river-overflow scenario considering: a) handrails
 651 implementation; b) handrails+raised platform implementation. The whole process evacuation curve for the original scenario is shown
 652 (line-two dots evacuation curve, in red, by including: minimum curve, as a dotted line; average curve, as line-two dots line; maximum
 653 curve, as a dashed line).

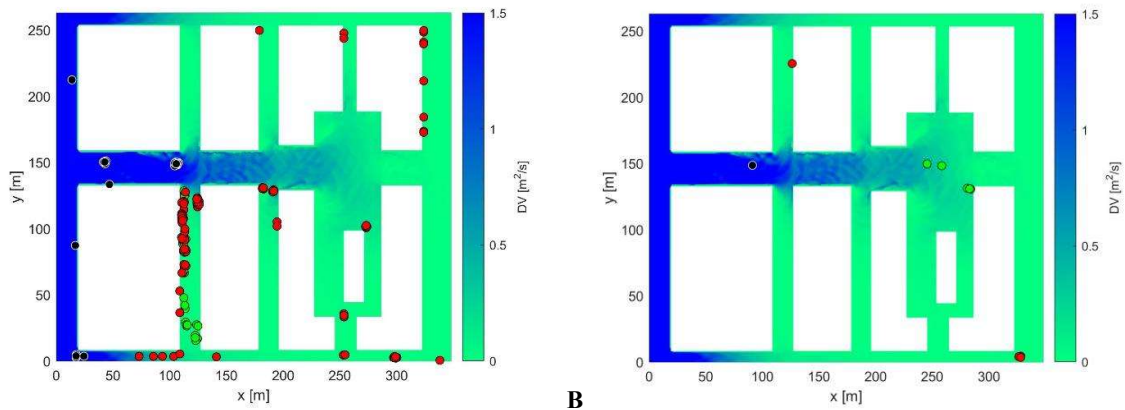
654

655
656
657

Table 8 Out-of-time evacuees P_O (and their characterization) in case of the implementation of handrails (H) and handrails+raised platform (H+P), according to the KPIs in Section 2.2.1. Percentage values are calculated with respect to the main or secondary related conditions.

Main condition	Secondary conditions	P_O (st. dev.)[per- sons]		$P_{O,\%}$ (st. dev.) [%]		$P_{O,la} - P_{O,sp} - P_{O,ca}$ [%]	
		<i>H</i>	<i>H+P</i>	<i>H</i>	<i>H+P</i>	<i>H</i>	<i>H+P</i>
all		157 (3)	11 (3)	52 (1)	4 (1)	69-31-0	67-33-0
evacuees who stop upstream (streets E and M) because of floodwater conditions (e.g. stability loss)		16 (1)	1 (1)	10 (1)	9 (9)	100-0-0	100-0-0
total number of evacuees located downstream		141 (2)	10 (2)	90 (1)	91 (18)	65-35-0	64-36-0
	evacuees who stop in the main street (streets K, L, A0)	25 (1)	6 (1)	18 (1)	60 (10)	32-68-0	17-83-0
	evacuees who stop near safe area 3	8 (0)	0 (0)	6 (0)	0 (0)	0-0-0	0-0-0
	evacuees who stop near a downstream safe area	9 (1)	7 (1)	6 (1)	70 (10)	100-0-0	100-0-0
	evacuees who stop in the square (square P-p1-p2)	15 (0)	5 (0)	11 (0)	50 (0)	0-0-0	0-0-0

658



659 **A** **B**
 660 **Figure 13.** Position of out-of-time evacuees at the end of the river-overflow simulations in case of: a) handrails implementation; b)
 661 handrails+raised platform implementation. Latecomers (red circles), spontaneously gathering evacuees (green circles), casualties (black
 662 circles) are shown on the DV map (scale on the right coloured bar).
 663

664 $R_{area,scen}$ and $R_{street,scen}$ proposed in Table 9 and Figure 14 are evaluated for the *original* and *risk reduction scenarios*.
 665 The floodwater conditions are the same in the three scenarios (see $R_{DV,area,scen}$ in Table 9). The handrails+raised platform
 666 implementation scenario is the best solution since it:

- 667 1. is the less affected by data on *out-of-time evacuees* (see the lowest $R_{O,area,scen}$);
- 668 2. shows an increase in the crowding-related factor because the majority of evacuees can reach a safe area (see
 669 the highest $R_{cr,street,scen}$);
- 670 3. is characterized by a $R_{area,scen, red-pre}$ reduction up to -54%.

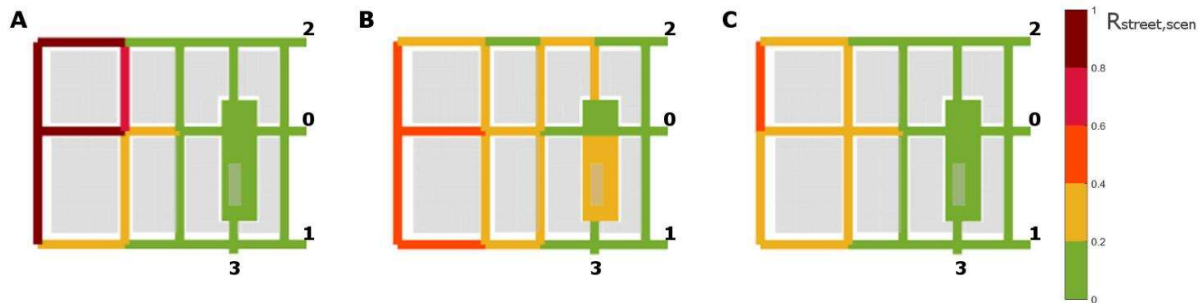
671
 672 **Table 9** Risk index for the whole area ($R_{area,scen}$) and the related influencing factors, by comparing river-overflow conditions in the
 673 original scenario with the handrails implementation and handrails+raised platform scenarios.

Scenario	$R_{O,area,scen}$	$R_{DV,area,scen}$	$R_{cr,area,scen}$	$R_{area,scen}$
Original scenario	0.85	1.00	0.64	0.89
Handrails implementation	0.26	1.00	0.69	0.53
Handrails+Raised platform implementation	0.02	1.00	1.00	0.41

674
 675 **Figure 14** graphically summarizes the risk of each street in the reference scenarios. $R_{DV,street,scen}$ values are always equal
 676 because of the same flood scenario (compare to supplementary material: S5 data). The results confirm the same conclu-
 677 sions offered for $R_{area,scen}$. Some downstream outdoor spaces (e.g. square p2) are affected by the presence of *out-of-time*

678 evacuees also in the risk reduction scenarios (see Figure 13). As a result, the overall risk of such spaces increases, but
679 casualties are not noticed here.

680



681

682 **Figure 14.** $R_{street,scen}$ representation by considering the river-overflow conditions in: a) the original scenario; b) handrails implementa-
683 tion; c) handrails+raised platform implementation. Buildings (light grey blocks) and safe area codes are supplied. The KPI scale is
684 shown by the colour map (0.2 ranges discretization). Raw data are shown by supplementary material: S5.

685

686 4 Discussion

687 The methodology application and the analysis of simulation results underline the general capabilities of the behavioural
688 design-based methodology and some rules to design risk reduction strategies for the outdoor built environment against
689 flood risk. For each of these key findings, specific case study outcomes are also provided.

690 The following capabilities of the simulation-based methodology could be highlighted:

- 691 • *Providing simulations on the current probable scenarios by including evacuation representation is useful to un-
692 derstand the dynamics of the emergency conditions over space and time from a holistic perspective.* According to
693 the proposed KPIs, the different flood scenarios are useful to individuate the best risk-reduction strategy to be
694 implemented. In fact, the proposed KPIs account for most of the effects of evacuation behaviours. *Meanwhile,
695 they focus on the outdoor built environment and its composing parts, which are pivotal elements for the evacuees’
696 safety during urban floods.* Such approach could be integrated into models based on Life Safety and Hazard or
697 AHP-based risk rating metrics (e.g. [10,11,22,34,54,62]) to include aspects such as (a) the evacuation curve/flows,
698 (b) the use of open spaces, and (c) the presence of spontaneous gathering areas. *Thus, the assessment of each part
699 of the built environment could be performed.* Concerning the specificities of the case study, the simulation results
700 show that the river-overflow scenario is riskier for the evacuees in the outdoor built environment if compared to

701 the considered levee-failure scenario. The main causes are due to the combination of the initial critical conditions
702 in floodwaters levels and their related quick-spreading in the urban layout, which brings evacuees to stop moving
703 (i.e. provoking casualties);

704 • *Effects of evacuees' attraction and gathering towards the nearest "safe" area is useful to identify where the res-*
705 *cuers' action should be focused to support the exposed evacuees.* In a regular urban environment, evacuees should
706 tend to move towards the outdoor areas that are orthogonally placed in respect to the main floodwater flows,
707 because of the local safer conditions in terms of floodwater levels. Thus, solutions aimed at collecting them in
708 such areas are recommended. Handrails can increase the safety of evacuees while moving towards these **areas**.
709 **Anyway, handrails** cannot completely improve the number of evacuees arriving at the safe areas themselves. Con-
710 cerning the case study, the majority of evacuees gathers in the upstream orthogonal streets instead of in the down-
711 stream ones because of the specific domain conditions.

712 Furthermore, from a modelling perspective, **the adopted approach takes advantage of** micro-scale and behavioural
713 design-based modelling criteria **to firstly consider both** pedestrian traffic and fatalities estimations [22,62]. **It also** seems
714 to overcome current limitations on experimental-based behaviours shown by many existing models (e.g.
715 [10,11,18,22,34,54,62]). In particular, the proposed evacuation model includes rules for: **(a)** spontaneous path selection
716 (moving towards areas with lower floodwater levels) and gathering behaviours; **(b)** coming-and-going behaviours; **(c)**
717 **attraction** towards immobile objects such as buildings, fences, handrails. Furthermore, the effects of such behaviours are
718 innovatively investigated at the micro-scale, that is considering each individual and each street or square in the built
719 environment. **The related overall** impact at the macro-scale **can be hence assessed**.

720 **Nevertheless, some** limitations concerning individual features exist because the model relies on average adults' evac-
721 uation simulation to demonstrate the methodology capabilities. Future works should model evacuation speeds and human
722 body stability issues inducing fatalities according to the specific individual characteristics, such as mass, height, age,
723 gender, and other motion abilities, also thanking specific experimental works [21,22,38,49]. This work adopts insights of
724 handrails use in evacuation conditions, by homogeneously considering that evacuees cannot lose **stability** while using
725 them [21,35,37,44,45]. **Future** works to estimate the effective support of handrails for evacuees moving on foot in flood-
726 waters **will hence** enrich the simulation of individual speeds while using handrails. Considering body stability issues, a
727 generic form of water depth versus velocity curve in the Life Safety Model could be adopted to represent the related
728 additional uncertainties, by pursuing, for instance, a probabilistic approach [22,25,54]. Further evaluations concerning
729 different human body stability loss phenomena (buoyancy; body failure), also in the view of the other stability-affecting
730 factors (e.g. age, gender, weight, height) [22,35,50,51], should be provided. Based on local census databases or in-situ

731 surveys [24,42], probabilistic distributions of the exposed people will be used in future works, thus including all uncer-
732 tainties which concern individuals' features and positions within the built environment over the time.

733 About the application context, this work is mainly centred on a limited built environment (a square and the nearby
734 streets), although the proposed framework could be applied to wider urban areas, both in existing and new urban contexts.
735 Nevertheless, splitting the domain into sub-areas could be preferred to analyse homogeneous areas in terms of built envi-
736 ronment or hazard or exposure conditions, also depending on the position of the reference gathering areas. At the same
737 time, **other built** environments, such as underground ones, can take advantage of this behavioural design-based method-
738 ology. In this case, the composing elements of the underground spaces (e.g. corridors, staircases, platforms in case of
739 underground stations) can be assessed in terms of floodwater characterization and evacuation process **through** the same
740 simulation rules and KPIs proposed by this work.

741 Considering risk reduction solutions, for the first time at the authors' knowledge, this work focuses on the effectiveness
742 analysis of architectural interventions in the outdoor built environment to support exposed individuals during the flood
743 emergency [35,37,45]. In this sense, the work provides insights on a solution that is less investigated than traditional ones,
744 such as those relating to the positioning of gathering areas, implementation of early warning systems, and modifications
745 to the emergency path configurations [22,54]. Simulation results highlight the following rules for risk reduction strategies
746 considering their design by technicians of Local Authorities and Civil Defence bodies:

- 747 • *handrails implementation in the scenario can effectively reduce the overall risk of the whole area as a consequence*
748 *of no casualties in the number of evacuees* (human body stability effects are avoided since evacuees can be sup-
749 ported by handrails). Concerning the specificities of the case study, this reduction is equal to about -40% if as-
750 suming that evacuees supported by handrails cannot lose their stability under any floodwater conditions;
- 751 • *raised **platforms** can be distributed in the urban fabric to create safe areas where evacuees can gather and wait*
752 *for the rescuers' arrival*. Their position can be defined according to the simulation results in the *original scenario*.
753 Anyway, some general rules can relate to concentrating them in upstream streets and in orthogonal streets where
754 evacuees tend to spontaneously gather. More data on the effective dimension of raised platforms can be provided
755 according to the related scenario simulations. Concerning the specificities of the case study, the reduction of the
756 overall area risk is up to about -54% while combining the raised platform with the implementation of handrails
757 along the upstream streets.

758 Handrails and raised platforms can be architecturally integrated to provide new spaces and activities in the outdoor
759 built environment. **In this work, the** case study application **would like** to depict the general capabilities of such architec-
760 tural micro-scale interventions, giving some preliminary and not-exhaustive examples. Although the possible efforts for

761 their implementation in the outdoor built environment, the integration of handrails and raised platform into the emergency
762 plan could reduce the residual risk due to possible lacks in warning systems implementation and functioning [84–86],
763 such as those due to lacks in the system organization or in the data operation or possible failures of the systems. They
764 could support also evacuees who could perform unsafe behaviours also if they are warned about the flood arrival (e.g.
765 time-wasting activities, selection of the wrong evacuation paths) [37].

766 Finally, the demonstration of the methodology capabilities underlines how stakeholders and planners can take ad-
767 vantage of **behavioural design-based** outcomes. **They can analyse** different event scenarios and **test** the effectiveness of
768 other kinds of risk reduction strategies, such as:

- 769 1. *macro-scale interventions*, e.g.: (a) early warning systems to alert the population and speed up the evacuation
770 before the critical conditions are reached; (b) drainage systems to limit the floodwater impacts on the evacu-
771 ation process;
- 772 2. *micro-scale solutions*, e.g.: (a) re-shaping of urban spaces to include architectural elements to support the
773 individuals; (b) evacuation guidance systems to point out the correct evacuation direction to the safer areas in
774 the urban fabric; (c) intervention on spaces that can host mass-gathering events; (d) urban spaces requalifica-
775 tion **using** architectural elements that could improve safety but could be also used in normal fruition condi-
776 tions²;
- 777 3. *emergency management strategies*, i.e.: (a) evacuation plan communication to people to improve their pre-
778 paredness and awareness; (b) gathering areas location according to micro-scale solutions.

779 The model could be modified to represent specific aspects and behavioural issues altering the decision model, the
780 pedestrian traffic model or the fatalities model depending on the considered solution.

781

782 **5 Conclusions**

783 Increasing the resilience of our communities against flood risk in the built environment should take advantage of the
784 evaluation of evacuees' behaviours and choices, especially if considering the initial phases of a flood emergency, i.e.
785 evacuation. In this sense, analyses on the outdoor built environment are key elements for evacuees' safety, **considering**
786 that evacuees can move in flood-affected scenarios. Simulation-based tools and methods can effectively evaluate the risk
787 for the exposed evacuees and the built environment from a holistic perspective. On this basis, **successful** risk reduction
788 strategies can be proposed to increase the resistance and resilience of the existing built environments **as long as they can:**

789 (a) effectively support evacuees to be safe during the emergency; (b) avoid additional threats; (c) lead evacuees to “cor-
790 rectly” behave in these critical emergency phases; (d) be easy-to-implement; (e) be integrated with the normal fruition of
791 the built environment also in non-disaster conditions.

792 Starting from this standpoint, this work proposes a micro-scale and behavioural design-based methodology to assess
793 the risk in outdoor built environments. **The methodology is used to** propose effective risk reduction solutions and then to
794 evaluate their effectiveness. **It** is holistic since it: (a) **is** based on the joint representation of floodwater hydrodynamics
795 and evacuation process; (b) combines critical descriptors of these two aspects into merged KPIs for risk assessment.

796 An existing experimental-based flood evacuation simulator is used to represent the emergency conditions and then to
797 provide data for the KPIs. The application to a case-study demonstrates the method capabilities in: (a) identifying risks
798 for evacuees due to the individual-floodwater-built environment interactions starting from the micro-scale behavioural
799 phenomena; (b) assessing the risk at the micro (i.e. street, square) and macro (i.e. whole outdoor built environment)-
800 scales; (c) comparing different flood scenarios, both including hydrodynamic and evacuation.-related standpoints; (d)
801 proposing and evaluating risk reduction actions, by mainly focusing the attention on architecturally-integrated elements
802 (e.g.: platforms, handrails) in high-risk outdoor spaces.

803 Risk evaluations and safety levels comparisons are possible through the proposed KPIs. Finally, simulation results also
804 trace some general remarks by focusing on the methodology (and KPIs) application, and on general criteria for imple-
805 menting the proposed **architecturally integrated elements** in the outdoor layout.

806 The methods and tools proposed by this work focus on evacuees’ behaviour and on the floodwater dynamic represen-
807 tation, but it does not consider the damages induced on the built environment itself. Thus, future activities should involve
808 the inclusion of the “built environment damage”-related factors (i.e. buildings, infrastructural elements, roads, and so on,
809 by also including drainage systems and sewers) as a function of floodwater spreading over the simulation time and space.
810 Moreover, the method should be applied to different typological scenarios to derive the related “typical” risk assessment
811 configuration, depending, **for instance**, on: the layout features; the possible flood events; the characterization of exposed
812 people in terms of emergency behaviours and risk awareness levels. Such application results will also encourage the
813 definition of best practices for increasing communities’ safety in the related outdoor built environment scenarios.

814 **6 Acknowledgement**

815 This work was supported by the “Building Resilience to flood Impact Deriving from Global warming in Europe –
816 BRIDGE” project, developed at Università Politecnica delle Marche.

817 **7 References**

- 818 [1] A.K. Mollah, S. Sadhukhan, P. Das, M.Z. Anis, A cost optimization model and solutions for shelter allocation
819 and relief distribution in flood scenario, *Int. J. Disaster Risk Reduct.* 31 (2018) 1187–1198.
820 <https://doi.org/10.1016/j.ijdr.2017.11.018>.
- 821 [2] K. Oubennaceur, K. Chokmani, M. Nastev, R. Lhissou, A. El Alem, Flood risk mapping for direct damage to
822 residential buildings in Quebec, Canada, *Int. J. Disaster Risk Reduct.* 33 (2019) 44–54.
823 <https://doi.org/10.1016/j.ijdr.2018.09.007>.
- 824 [3] D. Serre, C. Heinzlef, Assessing and mapping urban resilience to floods with respect to cascading effects through
825 critical infrastructure networks, *Int. J. Disaster Risk Reduct.* 30 (2018) 235–243.
826 <https://doi.org/10.1016/j.ijdr.2018.02.018>.
- 827 [4] P. Marana, C. Eden, H. Eriksson, C. Grimes, J. Hernantes, S. Howick, L. Labaka, V. Latinos, R. Lindner, T.A.
828 Majchrzak, I. Pyrko, J. Radianti, A. Rankin, M. Sakurai, J.M. Sarriegi, N. Serrano, Towards a resilience
829 management guideline — Cities as a starting point for societal resilience, *Sustain. Cities Soc.* 48 (2019) 101531.
830 <https://doi.org/10.1016/j.scs.2019.101531>.
- 831 [5] G. Cerè, Y. Rezgui, W. Zhao, Critical review of existing built environment resilience frameworks: Directions for
832 future research, *Int. J. Disaster Risk Reduct.* 25 (2017) 173–189. <https://doi.org/10.1016/j.ijdr.2017.09.018>.
- 833 [6] D. Molinari, F. Ballio, J. Handmer, S. Menoni, On the modeling of significance for flood damage assessment,
834 *Int. J. Disaster Risk Reduct.* 10 (2014) 381–391. <https://doi.org/10.1016/j.ijdr.2014.10.009>.
- 835 [7] J. Wu, M. Ye, X. Wang, E. Koks, Building Asset Value Mapping in Support of Flood Risk Assessments: A Case
836 Study of Shanghai, China, *Sustainability.* 11 (2019) 971. <https://doi.org/10.3390/su11040971>.
- 837 [8] C.E. Kontokosta, A. Malik, The Resilience to Emergencies and Disasters Index: Applying big data to benchmark
838 and validate neighborhood resilience capacity, *Sustain. Cities Soc.* 36 (2018) 272–285.
839 <https://doi.org/10.1016/j.scs.2017.10.025>.
- 840 [9] M.A.R. Shah, A. Rahman, S.H. Chowdhury, Sustainability assessment of flood mitigation projects: An innovative
841 decision support framework, *Int. J. Disaster Risk Reduct.* 23 (2017) 53–61.
842 <https://doi.org/10.1016/j.ijdr.2017.04.006>.
- 843 [10] H.-M. Lyu, W.-H. Zhou, S.-L. Shen, A.-N. Zhou, Inundation risk assessment of metro system using AHP and

- 844 TFN-AHP in Shenzhen, *Sustain. Cities Soc.* 56 (2020) 102103. <https://doi.org/10.1016/j.scs.2020.102103>.
- 845 [11] H.-M. Lyu, S.-L. Shen, A. Zhou, J. Yang, Perspectives for flood risk assessment and management for mega-city
846 metro system, *Tunn. Undergr. Sp. Technol.* 84 (2019) 31–44. <https://doi.org/10.1016/j.tust.2018.10.019>.
- 847 [12] E.L. French, S.J. Birchall, K. Landman, R.D. Brown, Designing public open space to support seismic resilience:
848 A systematic review, *Int. J. Disaster Risk Reduct.* 34 (2019) 1–10. <https://doi.org/10.1016/j.ijdr.2018.11.001>.
- 849 [13] K. Rus, V. Kilar, D. Koren, Resilience assessment of complex urban systems to natural disasters: A new literature
850 review, *Int. J. Disaster Risk Reduct.* 31 (2018) 311–330. <https://doi.org/10.1016/j.ijdr.2018.05.015>.
- 851 [14] UNISDR, *Guidelines for Reducing Flood Losses*, United Nations - Headquarters (UN), 2002.
- 852 [15] P.J.G. Ribeiro, L.A. Pena Jardim Gonçalves, Urban resilience: A conceptual framework, *Sustain. Cities Soc.* 50
853 (2019) 101625. <https://doi.org/10.1016/j.scs.2019.101625>.
- 854 [16] K. Park, J. Won, Analysis on distribution characteristics of building use with risk zone classification based on
855 urban flood risk assessment, *Int. J. Disaster Risk Reduct.* 38 (2019) 101192.
856 <https://doi.org/10.1016/j.ijdr.2019.101192>.
- 857 [17] G. Bernardini, M. Postacchini, E. Quagliarini, M. Brocchini, C. Cianca, M. D’Orazio, A preliminary combined
858 simulation tool for the risk assessment of pedestrians’ flood-induced evacuation, *Environ. Model. Softw.* 96
859 (2017) 14–29. <https://doi.org/10.1016/j.envsoft.2017.06.007>.
- 860 [18] K. Matsuo, L. Natinia, F. Yamada, Flood and Evacuation Simulations for Urban Flooding, 5th Int. Conf. Flood
861 Manag. (2011) 391–398.
- 862 [19] K. Kim, P. Pant, E. Yamashita, Integrating travel demand modeling and flood hazard risk analysis for evacuation
863 and sheltering, *Int. J. Disaster Risk Reduct.* 31 (2018) 1177–1186. <https://doi.org/10.1016/j.ijdr.2017.10.025>.
- 864 [20] J.G. Leskens, M. Brugnach, A.Y. Hoekstra, W. Schuurmans, Why are decisions in flood disaster management so
865 poorly supported by information from flood models?, *Environ. Model. Softw.* 53 (2014) 53–61.
866 <https://doi.org/10.1016/j.envsoft.2013.11.003>.
- 867 [21] H.-K. Lee, W.-H. Hong, Y.-H. Lee, Experimental study on the influence of water depth on the evacuation speed
868 of elderly people in flood conditions, *Int. J. Disaster Risk Reduct.* 39 (2019) 101198.
869 <https://doi.org/10.1016/j.ijdr.2019.101198>.
- 870 [22] D. Lumbroso, M. Davison, Use of an agent-based model and Monte Carlo analysis to estimate the effectiveness

- 871 of emergency management interventions to reduce loss of life during extreme floods, *J. Flood Risk Manag.* 11
872 (2018) S419–S433. <https://doi.org/10.1111/jfr3.12230>.
- 873 [23] M. Di Mauro, D. Lumbroso, Hydrodynamic and loss of life modelling for the 1953 Canvey Island flood, in: *Flood*
874 *Risk Manag. Res. Pract.*, CRC Press, 2008; pp. 1117–1126. <https://doi.org/10.1201/9780203883020.ch131>.
- 875 [24] D. Lumbroso, W. Johnstone, K. De Bruijn, M. Di Mauro, B. Lence, A. Tagg, Modelling mass evacuations to
876 improve the emergency planning for floods in the UK, the Netherlands and North America, in: *Int. Conf. Emerg.*
877 *Prep. (InterCEPt), Challenges Mass Evacuation*, University of Birmingham, United Kingdom, 2010.
- 878 [25] M.J.P. Mens, M. van der Vat, D. Lumbroso, A comparison of evacuation models for flood event management
879 application on the Schelde and Thames Estuaries, in: P. Samuels, S. Huntington, W. Allsop, J. Harrop (Eds.),
880 *Flood Risk Manag. Res. Pract.*, CRC Press/Balkema, Leiden, The Netherlands, 2008; pp. 1109–1115.
- 881 [26] G. Bernardini, R. Lovreglio, E. Quagliarini, Proposing behavior-oriented strategies for earthquake emergency
882 evacuation: A behavioral data analysis from New Zealand, Italy and Japan, *Saf. Sci.* 116 (2019) 295–309.
883 <https://doi.org/10.1016/j.ssci.2019.03.023>.
- 884 [27] S. Yamashita, R. Watanabe, Y. Shimatani, Smart adaptation activities and measures against urban flood disasters,
885 *Sustain. Cities Soc.* 27 (2016) 175–184. <https://doi.org/10.1016/j.scs.2016.06.027>.
- 886 [28] D. Lumbroso, F. Vinet, Tools to Improve the Production of Emergency Plans for Floods: Are They Being Used
887 by the People that Need Them?, *J. Contingencies Cris. Manag.* 20 (2012) 149–165.
888 <https://doi.org/10.1111/j.1468-5973.2012.00665.x>.
- 889 [29] S. Soares-Frazaõ, J. Lhomme, V. Guinot, Y. Zech, Two-dimensional shallow-water model with porosity for urban
890 flood modelling, *J. Hydraul. Res.* 46 (2008) 45–64. <https://doi.org/10.1080/00221686.2008.9521842>.
- 891 [30] A. Paquier, E. Mignot, P.-H. Bazin, From Hydraulic Modelling to Urban Flood Risk, *Procedia Eng.* 115 (2015)
892 37–44. <https://doi.org/10.1016/j.proeng.2015.07.352>.
- 893 [31] H. Chanson, R. Brown, New criterion for the stability of a human body in floodwaters, *J. Hydraul. Res.* 53 (2015)
894 540–541. <https://doi.org/10.1080/00221686.2015.1054321>.
- 895 [32] S. Opper, P. Cinque, B. Davies, Timeline modelling of flood evacuation operations, *Procedia Eng.* 3 (2010) 175–
896 187. <https://doi.org/10.1016/j.proeng.2010.07.017>.
- 897 [33] N. Mishima, N. Miyamoto, Y. Taguchi, K. Kitagawa, Analysis of current two-way evacuation routes based on

- 898 residents' perceptions in a historic preservation area, *Int. J. Disaster Risk Reduct.* 8 (2014) 10–19.
899 <https://doi.org/10.1016/j.ijdr.2013.12.003>.
- 900 [34] H.-M. Lyu, W.-J. Sun, S.-L. Shen, A. Arulrajah, Flood risk assessment in metro systems of mega-cities using a
901 GIS-based modeling approach, *Sci. Total Environ.* 626 (2018) 1012–1025.
902 <https://doi.org/10.1016/j.scitotenv.2018.01.138>.
- 903 [35] H. Chanson, R. Brown, D. McIntosh, Human body stability in floodwaters: the 2011 flood in Brisbane CBD, in:
904 *Hydraul. Struct. Soc. - Eng. Challenges Extrem.*, The University of Queensland, 2014: pp. 1–9.
905 <https://doi.org/10.14264/uql.2014.48>.
- 906 [36] P. Hu, Q. Zhang, P. Shi, B. Chen, J. Fang, Flood-induced mortality across the globe: Spatiotemporal pattern and
907 influencing factors, *Sci. Total Environ.* 643 (2018) 171–182. <https://doi.org/10.1016/j.scitotenv.2018.06.197>.
- 908 [37] G. Bernardini, S. Camilli, E. Quagliarini, M. D'Orazio, Flooding risk in existing urban environment: from human
909 behavioral patterns to a microscopic simulation model, *Energy Procedia.* 134 (2017) 131–140.
910 <https://doi.org/10.1016/j.egypro.2017.09.549>.
- 911 [38] R.J. Cox, M.J. Shand, T.D. Blacka, Australian Rainfall & Runoff revision project 10: Appropriate safety criteria
912 for people, 2010. <https://doi.org/10.1038/103447b0>.
- 913 [39] S.Y. Schreider, D.I. Smith, A.J. Jakeman, Climate Change Impacts on Urban Flooding, *Clim. Change.* 47 (2000)
914 91–115. <https://doi.org/10.1023/a:1005621523177>.
- 915 [40] X. Jia, G. Morel, H. Martell-Flore, F. Hissel, J.-L. Batoz, Fuzzy logic based decision support for mass evacuations
916 of cities prone to coastal or river floods, *Environ. Model. Softw.* 85 (2016) 1–10.
917 <https://doi.org/10.1016/j.envsoft.2016.07.018>.
- 918 [41] H. Qi, M.S. Altinakar, A GIS-based decision support system for integrated flood management under uncertainty
919 with two dimensional numerical simulations, *Environ. Model. Softw.* 26 (2011) 817–821.
920 <https://doi.org/10.1016/j.envsoft.2010.11.006>.
- 921 [42] A. Nara, X. Yang, S. Ghanipoor Machiani, M.-H. Tsou, An integrated evacuation decision support system
922 framework with social perception analysis and dynamic population estimation, *Int. J. Disaster Risk Reduct.* 25
923 (2017) 190–201. <https://doi.org/10.1016/j.ijdr.2017.09.020>.
- 924 [43] R. Zhu, J. Lin, B. Becerik-Gerber, N. Li, Human-building-emergency interactions and their impact on emergency

- 925 response performance: A review of the state of the art, *Saf. Sci.* 127 (2020) 104691.
926 <https://doi.org/10.1016/j.ssci.2020.104691>.
- 927 [44] K. Kotani, T. Ishigaki, S. Suzuki, T. Asao, Y. Baba, K. Toda, Evaluation for emergency escape during stair
928 climbing in a simulated flood evacuation, in: 2012 Southeast Asian Netw. Ergon. Soc. Conf., IEEE, 2012; pp. 1–
929 5. <https://doi.org/10.1109/SEANES.2012.6299592>.
- 930 [45] Y. Baba, T. Ishigaki, K. Toda, Experimental Studies on Safety Evacuation From Underground Spaces Under
931 Inundated Situations, *J. JSCE.* 5 (2017) 269–278. https://doi.org/10.2208/journalofjsce.5.1_269.
- 932 [46] M. Balakhontceva, V. Karbovskii, A. Boukhanovsky, S. Sutulo, Multi-agent Simulation of Passenger Evacuation
933 from a Damaged Ship Under Storm Conditions, *Procedia Comput. Sci.* 80 (2016) 2455–2464.
934 <https://doi.org/10.1016/j.procs.2016.05.547>.
- 935 [47] Y. Zheng, X.-G. Li, B. Jia, R. Jiang, Simulation of pedestrians' evacuation dynamics with underground flood
936 spreading based on cellular automaton, *Simul. Model. Pract. Theory.* 94 (2019) 149–161.
937 <https://doi.org/10.1016/j.simpat.2019.03.001>.
- 938 [48] T. Ishigaki, Y. Onishi, Y. Asai, K. Toda, H. Shimada, Evacuation criteria during urban flooding in underground
939 space, 11th Int. Conf. Urban Drain. (2008) 7.
- 940 [49] G. Bernardini, E. Quagliarini, M. D'Orazio, M. Brocchini, Towards the simulation of flood evacuation in urban
941 scenarios: Experiments to estimate human motion speed in floodwaters, *Saf. Sci.* 123 (2020) 104563.
942 <https://doi.org/10.1016/j.ssci.2019.104563>.
- 943 [50] L. Milanesi, M. Pilotti, R. Ranzi, A conceptual model of people's vulnerability to floods, *Water Resour. Res.*, 51,
944 182–197, Doi10.1002/2014WR016172. (2015) 5375–5377. <https://doi.org/10.1002/2013WR014979.Reply>.
- 945 [51] H.U. Bae, K.M. Yun, J.Y. Yoon, N.H. Lim, Human stability with respect to overtopping flow on the breakwater,
946 *Int. J. Appl. Eng. Res.* 11 (2016) 111–119.
- 947 [52] M. Postacchini, G. Bernardini, M. D'Orazio, E. Quagliarini, Human stability during floods: Experimental tests
948 on a physical model simulating human body, *Saf. Sci.* 137 (2021) 105153.
949 <https://doi.org/10.1016/j.ssci.2020.105153>.
- 950 [53] A. Schadschneider, W. Klingsch, H. Klüpfel, T. Kretz, C. Rogsch, A. Seyfried, Evacuation Dynamics: Empirical
951 Results, Modeling and Applications, *Encycl. Complex. Syst. Sci.* (2009) 3142-3176 LA-English.

- 952 https://doi.org/10.1007/978-0-387-30440-3_187.
- 953 [54] M. Shirvani, G. Kesserwani, P. Richmond, Agent-based modelling of pedestrian responses during flood
954 emergency: mobility behavioural rules and implications for flood risk analysis, *J. Hydroinformatics*. 22 (2020)
955 1078–1092. <https://doi.org/10.2166/hydro.2020.031>.
- 956 [55] A. Veeraswamy, E.R. Galea, L. Filippidis, P.J. Lawrence, S. Haasanen, R.J. Gazzard, T.E.L. Smith, The
957 simulation of urban-scale evacuation scenarios with application to the Swinley forest fire, *Saf. Sci.* 102 (2018)
958 178–193. <https://doi.org/10.1016/j.ssci.2017.07.015>.
- 959 [56] H. Chu, J. Yu, J. Wen, M. Yi, Y. Chen, Emergency Evacuation Simulation and Management Optimization in
960 Urban Residential Communities, *Sustainability*. 11 (2019) 795. <https://doi.org/10.3390/su11030795>.
- 961 [57] A. Zlateski, M. Lucesoli, G. Bernardini, T.M. Ferreira, Integrating human behaviour and building vulnerability
962 for the assessment and mitigation of seismic risk in historic centres: Proposal of a holistic human-centred
963 simulation-based approach, *Int. J. Disaster Risk Reduct.* 43 (2020) 101392.
964 <https://doi.org/10.1016/j.ijdrr.2019.101392>.
- 965 [58] N. Wood, J. Jones, J. Peters, K. Richards, Pedestrian evacuation modeling to reduce vehicle use for distant
966 tsunami evacuations in Hawai‘i, *Int. J. Disaster Risk Reduct.* 28 (2018) 271–283.
967 <https://doi.org/10.1016/j.ijdrr.2018.03.009>.
- 968 [59] G. Lämmel, D. Grether, K. Nagel, The representation and implementation of time-dependent inundation in large-
969 scale microscopic evacuation simulations, *Transp. Res. Part C Emerg. Technol.* 18 (2010) 84–98.
970 <https://doi.org/10.1016/j.trc.2009.04.020>.
- 971 [60] S. Scheuer, D. Haase, V. Meyer, Towards a flood risk assessment ontology – Knowledge integration into a multi-
972 criteria risk assessment approach, *Comput. Environ. Urban Syst.* 37 (2013) 82–94.
973 <https://doi.org/10.1016/j.compenvurbsys.2012.07.007>.
- 974 [61] F. Dottori, R. Figueiredo, M.L. V. Martina, D. Molinari, A.R. Scorzini, INSYDE: a synthetic, probabilistic flood
975 damage model based on explicit cost analysis, *Nat. Hazards Earth Syst. Sci.* 16 (2016) 2577–2591.
976 <https://doi.org/10.5194/nhess-16-2577-2016>.
- 977 [62] L. Zhuo, D. Han, Agent-based modelling and flood risk management: A compendious literature review, *J. Hydrol.*
978 591 (2020) 125600. <https://doi.org/10.1016/j.jhydrol.2020.125600>.

- 979 [63] S.P. Simonovic, S. Ahmad, Computer-based Model for Flood Evacuation Emergency Planning, *Nat. Hazards*. 34
980 (2005) 25–51. <https://doi.org/10.1007/s11069-004-0785-x>.
- 981 [64] L. Melito, M. Postacchini, G. Darvini, M. Brocchini, Waves and currents at a river mouth: The role of
982 macrovortices, sub-grid turbulence and seabed friction, *Water (Switzerland)*. 10 (2018).
983 <https://doi.org/10.3390/w10050550>.
- 984 [65] D. Helbing, A.F. Johansson, Pedestrian, Crowd and Evacuation Dynamics, *Encycl. Complex. Syst. Sci.* 16 (2010)
985 6476–6495.
- 986 [66] T. Ishigaki, R. Kawanaka, Y. Onishi, H. Shimada, K. Toda, Y. Baba, Assessment of Safety on Evacuating Route
987 During Underground Flooding BT - *Advances in Water Resources and Hydraulic Engineering*, in: C. Zhang, H.
988 Tang (Eds.), Springer Berlin Heidelberg, Berlin, Heidelberg, 2009: pp. 141–146.
- 989 [67] E. Ronchi, E.D. Kuligowski, P.A. Reneke, R.D. Peacock, D. Nilsson, The Process of Verification and Validation
990 of Building Fire Evacuation Models, *NIST Tech. Note*. 1822 (2013).
- 991 [68] M. Hashemi, A.A. Alesheikh, A GIS-based earthquake damage assessment and settlement methodology, *Soil
992 Dyn. Earthq. Eng.* 31 (2011) 1607–1617. <https://doi.org/10.1016/j.soildyn.2011.07.003>.
- 993 [69] N. Emori, T. Izumi, Y. Nakatani, A Support System for Developing Tourist Evacuation Guidance, in: H.K. Kim,
994 M.A. Amouzegar, S. Ao (Eds.), *Trans. Eng. Technol.*, Springer Singapore, Singapore, 2016: pp. 15–28.
995 https://doi.org/10.1007/978-981-10-0551-0_2.
- 996 [70] M. Haghani, M. Sarvi, Crowd behaviour and motion: Empirical methods, *Transp. Res. Part B Methodol.* 107
997 (2018) 253–294. <https://doi.org/10.1016/J.TRB.2017.06.017>.
- 998 [71] M. D’Orazio, S. Longhi, P. Olivetti, G. Bernardini, Design and experimental evaluation of an interactive system
999 for pre-movement time reduction in case of fire, *Autom. Constr.* 52 (2015) 16–28.
1000 <https://doi.org/10.1016/j.autcon.2015.02.015>.
- 1001 [72] T. Korhonen, S. Hostikka, *Fire Dynamics Simulator with Evacuation: FDS + Evac Technical Reference and
1002 User’s Guide*, 2010.
- 1003 [73] L. Taneja, N.B. Bolia, Network redesign for efficient crowd flow and evacuation, *Appl. Math. Model.* (2017).
1004 <https://doi.org/10.1016/j.apm.2017.08.030>.
- 1005 [74] V. Pillac, P. Van Hentenryck, C. Even, A conflict-based path-generation heuristic for evacuation planning,

- 1006 Transp. Res. Part B Methodol. 83 (2016) 136–150. <https://doi.org/10.1016/j.trb.2015.09.008>.
- 1007 [75] M. Sasabe, K. Fujii, S. Kasahara, Road network risk analysis considering people flow under ordinary and
1008 evacuation situations, Environ. Plan. B Urban Anal. City Sci. (2018) 239980831880294.
1009 <https://doi.org/10.1177/2399808318802940>.
- 1010 [76] D. Kazantzidou-Firtinidou, C. Gountromichou, N.C. Kyriakides, P. Liassides, K. Hadjigeorgiou, SEISMIC RISK
1011 ASSESSMENT AS A BASIC TOOL FOR EMERGENCY PLANNING: “PACES” EU PROJECT, WIT Trans.
1012 Built Environ. 173 (2017) 43–54. <https://doi.org/10.2495/DMAN170051>.
- 1013 [77] T.L. Saaty, The Analytic Hierarchy Process, New York, NY, USA, 1980. <https://doi.org/0070543712>.
- 1014 [78] A. Shayannejad, B. Abedini Angerabi, Earthquake Vulnerability Assessment in urban areas using MCDM, Int.
1015 Rev. Spat. Plan. Sustain. Dev. 2 (2014) 39–51. https://doi.org/10.14246/irspds.2.2_39.
- 1016 [79] E. Quagliarini, G. Bernardini, S. Santarelli, M. Lucesoli, Evacuation paths in historic city centres: A holistic
1017 methodology for assessing their seismic risk, Int. J. Disaster Risk Reduct. 31 (2018) 698–710.
1018 <https://doi.org/10.1016/j.ijdrr.2018.07.010>.
- 1019 [80] M. Brocchini, J. Calantoni, M. Postacchini, A. Sheremet, T. Staples, J. Smith, A.H. Reed, E.F. Braithwaite, C.
1020 Lorenzoni, A. Russo, S. Corvaro, A. Mancinelli, L. Soldini, Comparison between the wintertime and summertime
1021 dynamics of the Misa River estuary, Mar. Geol. 385 (2017) 27–40. <https://doi.org/10.1016/j.margeo.2016.12.005>.
- 1022 [81] Ministry of Interior (Italy), DM 03/08/2015: Fire safety criteria (Approvazione di norme tecniche di prevenzione
1023 incendi, ai sensi dell’articolo 15 del decreto legislativo 8 marzo 2006, n. 139.), 2015.
- 1024 [82] T. Klüpfel, H. Meyer-König, PedGo Guardian: an assistant for evacuation decision making, in: U. Weidmann, U.
1025 Kirsch, M. Schreckenber (Eds.), Pedestr. Evacuation Dyn. 2012, Springer International Publishing, 2014: pp.
1026 445–454.
- 1027 [83] A. Johansson, D. Helbing, H.Z. Al-Abideen, S. Al-Bosta, From Crowd Dynamics to Crowd Safety: A Video-
1028 Based Analysis, Adv. Complex Syst. 11 (2008) 497–527.
- 1029 [84] S.H.M. Fakhruddin, A. Kawasaki, M.S. Babel, Community responses to flood early warning system: Case study
1030 in Kaijuri Union, Bangladesh, Int. J. Disaster Risk Reduct. 14 (2015) 323–331.
1031 <https://doi.org/10.1016/j.ijdrr.2015.08.004>.
- 1032 [85] Q. Fan, Z. Tian, W. Wang, Study on Risk Assessment and Early Warning of Flood-Affected Areas when a Dam

1033 Break Occurs in a Mountain River, *Water*. 10 (2018) 1369. <https://doi.org/10.3390/w10101369>.

1034 [86] J. Cools, D. Innocenti, S. O'Brien, Lessons from flood early warning systems, *Environ. Sci. Policy*. 58 (2016)
1035 117–122. <https://doi.org/10.1016/j.envsci.2016.01.006>.

1036 [87] R. Briganti, A. Torres-Freyermuth, T.E. Baldock, M. Brocchini, N. Dodd, T.-J. Hsu, Z. Jiang, Y. Kim, J.C.
1037 Pintado-Patiño, M. Postacchini, Advances in numerical modelling of swash zone dynamics, *Coast. Eng.* 115
1038 (2016) 26–41. <https://doi.org/10.1016/j.coastaleng.2016.05.001>.

1039

1040 **Appendix A: FlooPEDS model description**

1041 The Flooding Pedestrians' Evacuation Dynamics Simulator (FlooPEDS) was adopted in this work for joint hydrody-
1042 namic and evacuation simulation purposes [17]. All the notations of the model are reported and described in Table A.1.

1043 The hydrodynamic model is based on the solution of the Nonlinear Shallow Water Equations [87]. The NSW solver
1044 has been validated during the last decades over very different shallow-water contexts (e.g. [64,87]). Its verification in an
1045 urban environment during a historical event (in combination with the evacuation/behavioural model) is reported in the
1046 original work about FlooPEDS [17]. NSWs consist of a continuity equation and two momentum-conservation equations
1047 along x and y , as shown in Equations 1, 2 and 3:

$$1048 \quad D_{,t} + (uD)_{,x} + (vD)_{,y} = 0 \quad (2)$$

$$1049 \quad u_{,t} + uu_{,x} + vu_{,y} + gD_{,x} = gh_{,x} - B_x \quad (3)$$

$$1050 \quad v_{,t} + uv_{,x} + vv_{,y} + gD_{,y} = gh_{,y} - B_y \quad (4)$$

1051

1052 These are used for the description of depth-averaged flows, where: commas represent partial differentiation, (x,y,z) are
1053 the orthogonal Cartesian coordinates; (u, v) is the depth-averaged velocity vector, with modulus V [m/s]; the total water
1054 depth D is made of the bed level h and the instantaneous water surface level $\eta = D - h$; the Chezy-type bottom friction
1055 is represented by B_x and B_y [64]. The simulated scenarios are represented using a 3D mesh with a **given constant** spatial
1056 resolution. For the case study of Section 2.3, the mesh covers an area of 350m by 265m as shown in Figure 2, in which
1057 each rectangular cell is characterized by a spatial resolution of $(\Delta x, \Delta y)=(0.8, 0.5)$ m. Each building block is represented
1058 as a discrete rectangular-shaped obstacle. For each cell not covering the building blocks, the hydrodynamic simulator

1059 provides the time evolution of water depth $D(x,y,t)$ and depth-averaged flow speed $V(x,y,t)$. These both provide the specific force per unit width $M(x,y,t)$ [m^3/m] and the human body stability conditions $DV(x,y,t)$ [m^2/s] as discussed in Section 2.1 [18,35,48].

1062 The micro-scale evacuation model combines: (a) an Agent-Based Model (ABM) to describe intentional issues of the evacuees in terms of behavioural patterns [37]; and (b) a Social Force Model (SFM) [65] to describe the motion process as the combination of attractive and repulsive forces connected to the behavioural patterns of the ABM. Each simulated pedestrian moves in the designed 2D continuous space and tries to reach a safe area. His/her motion is influenced by the surrounding $D(x,y,t)$, $V(x,y,t)$ and $M(x,y,t)$ values, that are calculated by the hydrodynamic simulator. The evacuation motion is solved within a maximum evacuation time, which is fixed according to the hydrodynamic simulation conditions.

1068 It was assumed that all the individuals know the position of the safe area. Thus, each simulated agent selects its evacuation path to minimize the distance towards the safe area and the risk due to floodwater conditions (i.e., in terms of M). Paths selection decision can be performed at the initial position point and at the crossroads or in other decisional points (e.g. plano-altimetric variations of the urban layout). To this end, in such positions, he/she evaluates the local conditions of the possible paths to be selected (in terms of M and distance to the safe area). If the shortest path is the one with the lower M value, he/she moves toward this path. Otherwise, he/she moves towards another path. As a result, a difference can exist between the safe area **selected at the start of the evacuation**, and **the safe area gained at the end of the process**.

1075 The path selection influences the evacuation direction since it steers the individual's SFM-based drive-to-target force \vec{O}_g [N]. Then, his/her preferred evacuation speed $v_{pref,i}(x,y,t)$ varies over time and space depending on $M(x,y,t)$, as shown by Equation 5 which is based on previous experimental results [37].

1078

$$1079 \quad v_{pref,i}(x,y,t) = 0.52 M(x,y,t)^{-0.11} \quad (5)$$

1080

1081 \vec{O}_g is the result of attractive and repulsive forces that modify his/her final local evacuation direction. Attractive forces are activated towards [17]: unmovable obstacles (i.e. buildings, fences and other street furniture, handrails) that can support the individual's motion in floodwaters (see $\vec{F}_{attr,w}$ [N] in Equation 6); other surrounding individuals, because of social identification and group phenomena [65]. Repulsive forces $\vec{F}_{rep,w}$ [N] are aimed at avoiding individual-individual and built elements-individual overlapping [65].

1086

$$1087 \quad \vec{F}_{attr,w}(t) = F_w \frac{d_w - R_i}{d_{w,max}} \vec{t}_w \quad \text{if } d_w < d_{w,max} \text{ , } F_w \vec{t}_w \quad \text{elsewhere} \quad (6)$$

1088

1089 Finally, Equation 7 summarizes the SFM-based equation to solve the motion of each evacuee, step by step during the
1090 simulation time. Some random variations in the behaviours could be described by the term $\overline{\varepsilon(t)}$ [N] [65].

1091

$$1092 \quad m_i \frac{d\overline{v_i(t)}}{dt} = \overline{O_g(t)} + \sum \overline{F_{rep,i}(t)} + \sum \overline{F_{re,w}(t)} + \sum \overline{F_{attr,i}(t)} + \sum \overline{F_{attr,w}(t)} + \overline{\varepsilon(t)} \quad (7)$$

1093

1094 The evacuation ends if the individual:

- 1095 • reaches a safe area (*arrived evacuees*) or at the end of the simulation time, if the individual is still moving and
1096 he/she is not able to reach a safe area within the maximum simulation time because of his/her evacuation path
1097 or speed. Such *latecomers* can be affected, for instance, by the interactions with other pedestrians and/or with
1098 speed-decreasing floodwaters conditions;
- 1099 • moves along the same path more than 1 time, since M values of surrounding paths are worse than the ones of the
1100 selected path. According to this experimental-based behaviour, he/she can spontaneously gather with surround-
1101 ing individuals because of $\overline{F_{attr,i}}$ (*spontaneously gathering evacuees*);
- 1102 • stops moving because of critical surrounding conditions, i.e. in case of body stability loss ($DV > 1.20 \text{ m}^2/\text{s}$)
1103 [31,38]. Such conditions could eventually provoke life threats by considering adult pedestrians (*casualties*). In
1104 addition, $D(x,y,t) < 1.2 \text{ m/s}$ and $V(x,y,t) < 3.2 \text{ m/s}$ are considered as limiting values for adults in good conditions
1105 having a height (h_i) and mass (m_i) product $h_i m_i > 50$ [38].

1106 Equation 6 is solved for $dt=0.1\text{s}$, by using the Euler's method in a separate way for x and y axes, to update each
1107 simulated individual's position. According to Equation 6 and Equation 7, the following main variables setup was used
1108 for the evacuation simulator [17]: $m_i=80\text{kg}$ (however, $h_i m_i > 50$) and $R_i=0.35\text{m}$ (to represent an average adult evacuee);
1109 $F_w=300\text{N}$ and $d_{w,max}=9\text{m}$; $\varepsilon(t)=0\text{N}$.

1110

1111

Table A.1 Modeling notations.

Symbol	Measure	Description
B_x, B_y	ms^{-2}	Bottom friction terms
D	m	Total water depth
d_w	m	Actual distance between pedestrian i and obstacle w

$d_{w,max}$	m	Maximum distance of activation for attractive forces between the pedestrian and the unmovable obstacle
$\vec{F}_{attr,i}, \vec{F}_{attr,w}$	(modulus) N	Attractive forces for group interactions and for fixed obstacles influence
$\vec{F}_{rep,i}, \vec{F}_{rep,w}$	(modulus) N	Repulsive force from other pedestrians and from obstacles
F_w	N	Constant parameter for maximum attraction force between a pedestrian and the unmovable obstacle
g	9.81 m/s ²	gravity acceleration
h	m	Bottom vertical position
i, j, w	-	Subscripts for: the pedestrian subject of valuation; other pedestrians; an obstacle
\vec{l}_w	-	Versor between the current pedestrian i position and the unmovable obstacle which attract the pedestrian
$M(x,y,t)$	m ³ /m	specific force per unit width, which varies over space (x and y coordinates) and time (t)
m_i	kg	Pedestrian mass
$\vec{O}_g(t)$	(modulus) N	Drive-to-target force
R_i	m	Radius of pedestrian i , that is the distance between his/her barycentre and his/her shoulder, thus considering an ideal circle circumscribing the individual on a plan view
t, dt	s	Time in motion simulation evaluation, gap between two different motion simulation evaluation
u	m/s	Depth-averaged streamwise (x -directed) velocity
v	m/s	Depth-averaged crossflow (y -directed) velocity
V	m/s	Modulus of the Depth-averaged velocity vector
$v_{pref,i}(x, y, t)$	m/s	Preferred individuals' speed for isolated pedestrian i in floodwaters (in "those" conditions and without considering other pedestrians)
$\vec{v}(t)$	(modulus) m/s	Actual velocity of the pedestrian
$\vec{\varepsilon}(t)$	(modulus) N	Gaussian error due to possibility of different evacuees' behaviours and features

η	m	Instantaneous water surface level
$\vec{\eta}_{iw}$	-	Unit vector pointing from i to w used for repulsive forces calculus

1112 **Appendix B: KPIs notations**

KPI symbol	Measure	KPI Description
<i>difference in arriving evacuees</i>	[%]	percentage difference between the number of evacuees reaching the safe area at the simulation end and the one of evacuees “initially choosing” the safe area
$F_e : F_{e,0.05}, F_{e,0.50}, F_{e,0.95}$	[persons/s]	effective average flow of evacuees arrived in a safe area: flows for $P_e=5\%$, $P_e=50\%$ and $P_e=95\%$
$P_O, P_{O,street}$	[persons]	number of out-of-time evacuees (including casualties); number of out-of-time evacuees (including casualties) for a certain street
$P_{O,\%}, P_{O,street,\%}$	[%]	percentage of out-of-time evacuees (including casualties) in respect to number of exposed people in the outdoor built environment; value referred to a certain street
$P_{O,la}, P_{O,la,street}$	[%]	percentages of latecomers in respect to P_O ; value for a certain street
$P_{O,sp}, P_{O,sp,street}$	[%]	percentages of spontaneously gathering evacuees in respect to P_O ; value for a certain street
$P_{O,ca}, P_{O,ca,street}$	[%]	percentages of casualties in respect to P_O ; value for a certain street
P_e	[persons]	number of evacuees arrived in a safe area within the simulation time
$P_{e,\%}$	[%]	percentage of evacuees arrived in a safe area within the simulation time in respect to the number of exposed people in the outdoor built environment
$P_{cr,street}, P_{cr,street,\%}$	[persons]	street crowding (how many evacuees go through a given street in the urban layout while evacuating); percentage value calculated in respect of the maximum $P_{cr,street}$ value within the simulated area
$R_{area,scen}$	-	the risk of the whole <i>area</i> in a given scenario <i>scen</i>
$R_{street,scen}$	-	the risk of a single <i>street</i> (or square) in a given <i>scen</i>
R_{street}	-	the risk of a single <i>street</i> (or square) in comparison to other streets (squares) in a given scenario

$R_{O,area,scen}$ $,R_{O,street,scen} , R_{O,street}$	-	risk for out-of-time evacuees: for the whole area in the given scenario, for the given in the considered scenario, on the given street
$R_{DV,area,scen} ,$ $R_{DV,street,scen} ,$ $R_{DV,street}$	-	risk due to the floodwater level: for the whole area in the given scenario, for the street in the given scenario, on the given street
$R_{cr,area,scen} ,$ $R_{cr,street,scen} , R_{cr,street}$	-	<i>crowding risk index on the area</i> : for the whole area in the considered scenario, for the street in the considered scenario, on the considered street
$T_e : T_{e,0.05} , T_{e,0.50} ,$ $T_{e,0.95}$	[s]	evacuation time: evacuation time for $P_e=5\%$, $P_e=50\%$ and $P_e=95\%$
Weights in AHP	Measure	Weights Description
w_O	-	out-of-time evacuees-related weight in the level 1 AHP application (related to $R_{O,area,scen} , R_{O,street,scen}$ and $R_{O,street}$)
w_{DV}	-	DV-related weight in the level 1 AHP application (related to $R_{DV,area,scen} , R_{DV,street,scen}$ and $R_{DV,street}$)
w_{cr}	-	crowding-related weight in the level 1 AHP application (related to $R_{cr,area,scen} , R_{cr,street,scen}$ and $R_{cr,street}$)
w_{sp} , w_{la} , w_{ca}	-	weights related to spontaneously gathering evacuees, latecomers, casualties to be applied in the level 2 AHP application for the components of $R_{O,area,scen} , R_{O,street,scen}$ and $R_{O,street}$

1113 Appendix C: Risk indices relating to the built environment

1114 The following paragraphs describe the definition of the area risk-related KPIs, which represent the overall risk condi-
1115 tions for the whole simulation area or for a part of it:

- 1116 • the risk of the whole area $R_{area,scen}$ [-] considers different scenarios to compare the risks of the whole area in
1117 each of them (section C.1);
- 1118 • the risk of a single street (or square) $R_{street,scen}$ [-] considers different scenarios to compare the risks of the street
1119 in each of them (section C.2);
- 1120 • the risk of a single street (or square) in comparison to other streets (squares) R_{street} considers the conditions
1121 within the same given scenario [-] (section C.3).

1122 All these KPIs were based on a **two-level** Decision Hierarchy, as shown by Table C1. The weight estimation was
 1123 performed through the open-source tool AHP Online System⁵. The first level is **composed of** factors (in order of im-
 1124 portance):

- 1125 (a) related to the *out-of-time evacuees* (“how many evacuees cannot reach a safe area?”). The associate weight is w_O
 1126 [-]. This factor was associated with 3 second-level variables, depending on the reasons inducing the evacuees to
 1127 stop out of a safe area (compare to Section 2.2.1). In order of importance, they are: *casualties* (w_{ca}), because they
 1128 represent evacuees who cannot be saved at the end of the emergency; *latecomers* (w_{la}), since they can still move
 1129 at the end of the simulation; *spontaneously gathering evacuees* (w_{sp}), since they are located in areas where *DV*
 1130 conditions are not critical at all;
- 1131 (b) related to the floodwater risk levels (“how much the flood is critical?”), in terms of *DV*, since it affects the human
 1132 body stability. This factor has no second-level variable. The associate weight is w_{DV} [-];
- 1133 (c) related to the use of the urban layout and of the paths (“where evacuees move?”), or rather on the overall crowding
 1134 conditions along the streets. This factor has no second-level variable. It is the least relevant because it just outlines
 1135 the possibility of individual-individual interactions along the paths and the probable exposure to particular *DV*
 1136 levels during the whole **evacuation** process⁶. The associate weight is w_{cr} [-].

1137

1138 **Table C1** Decision hierarchy overview for the risk indices, by including principal eigenvalue and Ratio of Consistency evaluated
 1139 through the AHP application, for each level.

	Level 1	Level 2
Relative Risk Index	out-of-time evacuees-related: $w_O=0.604$	spontaneously gathering evacuees: $w_{sp}=0.073$
		latecomers: $w_{la}=0.200$
		casualties: $w_{ca}=0.727$
	<i>DV</i> -related: $w_{DV}=0.326$	-
	crowding-related: $w_{cr}=0.07$	-
Principal eigen value	3.006	3.009
<i>RC</i>	0.60%	1.00%

1140

⁵ <https://bpmmsg.com/ahp/ahp-hierarchy.php> (last access: 19/09/2019)

⁶ e.g. *DV*-related factors being equal in two parts of the same scenario, the less riskiest is the one with the lowest crowding level since evacuees can more freely move.

1141 **C.1 $R_{area,scen}$**

1142 Let consider different comparable scenarios to measure the risks of the whole area in each of them. For each scenario,
 1143 $R_{area,scen}$ was calculated according to Table C1 decision hierarchy, as shown by Equation C.1:

$$1144 R_{area,scen} = R_{O,area,scen} \cdot w_O + R_{DV,area,scen} \cdot w_{DV} + R_{cr,area,scen} \cdot w_{cr} = \left(\frac{P_{O,ca}}{P_{O,ca,max,scen}} \cdot w_{ca} + \frac{P_{O,la}}{P_{O,la,max,scen}} \cdot w_{la} + \right. \\ 1145 \left. \frac{P_{O,sp}}{P_{O,sp,max,scen}} \cdot w_{sp} \right) \cdot w_O + \frac{DV_{area,max}}{DV_{area,max,scen}} \cdot w_{DV} + \frac{P_{cr,area,max}}{P_{cr,area,max,scen}} \cdot w_{cr} \quad (C.1)$$

1146 where *max* refers to the maximum value in the area in the given scenario, and *max,scen* refers to the maximum value
 1147 in all the comparable scenarios.

1148 **C.2 $R_{street,scen}$**

1149 Let consider different comparable scenarios to measure the risks of a given street in each of them. For each scenario,
 1150 $R_{street,scen}$ was calculated according to Table C1 decision hierarchy, as shown by Equation C.2:

$$1151 R_{street,scen} = R_{O,street,scen} \cdot w_O + R_{DV,street,scen} \cdot w_{DV} + R_{cr,street,scen} \cdot w_{cr} = \left(\frac{P_{O,ca,street}}{P_{O,ca,street,max,scen}} \cdot w_{ca} + \right. \\ 1152 \left. \frac{P_{O,la,street}}{P_{O,la,street,max,scen}} \cdot w_{la} + \frac{P_{O,sp,street}}{P_{O,sp,street,max,scen}} \cdot w_{sp} \right) \cdot w_O + \frac{DV_{street,max}}{DV_{area,max,scen}} \cdot w_{DV} + \frac{P_{cr,street}}{P_{cr,street,max,scen}} \cdot w_{cr} \quad (C.2)$$

1153 where, where *max* refers to the maximum value for the considered street in the given scenario, and *max,scen* refers to
 1154 the maximum value in all the comparable scenarios.

1155 **C.3 R_{street}**

1156 Let consider a certain scenario to compare the risks of the open spaces in the built environment (i.e. streets, squares).
 1157 For each open space (i.e. street) in the simulation area, R_{street} was calculated according to Table C1 decision hierarchy, as
 1158 shown by Equation C.3:

$$1159 R_{street} = R_{O,street} \cdot w_b + R_{DV,street} \cdot w_{DV} + R_{cr,street} \cdot w_{cr} = \left(\frac{P_{O,ca,street}}{P_{O,ca,street,max}} \cdot w_{ca} + \frac{P_{O,la,street}}{P_{O,la,street,max}} \cdot w_{la} + \right. \\ 1160 \left. \frac{P_{O,sp,street}}{P_{O,sp,street,max}} \cdot w_{sp} \right) \cdot w_O + \frac{DV_{street,max}}{DV_{area,max}} \cdot w_{DV} + \frac{P_{cr,street}}{P_{cr,street,max}} \cdot w_{cr} \quad (C.3)$$

1161 where *max* refers to the maximum value in the given scenario.